Linköping Studies in Science and Technology
Licentiate Thesis No. 1549

Modeling and Simulation of Microdialysis in the Deep Brain Structures

Elin Diczfalusy

Linköping University

Department of Biomedical Engineering
Linköping University

Linköping 2012

Modeling and simulation of microdialysis in the deep brain structures

Linköping Studies in Science and Technology
Licentiate Thesis No. 1549

Department of Biomedical Engineering
Linköping University
SE-581 85 Linköping, Sweden

This is a Swedish Licentiate Thesis. The Licentiate degree comprises 120 ECTS credits for postgraduate studies.

ISBN: 978-91-7519-805-7
ISSN: 0280-7971

Printed by LiU-Tryck Linköping, 2012

Abstract

Microdialysis is a method for monitoring of the local biochemical environment in a region of interest. The method uses a catheter, mimicking the function of a blood capillary, to sample substances from the surrounding medium through diffusion. A recent application for microdialysis is the sampling of neuroactive substances in the deep brain, or basal ganglia, during deep brain stimulation (DBS) for patients with Parkinson's disease. The basal ganglia consist of nuclei interconnected by chemical synapses, and it is hypothesized that the levels of neurotransmitter substances around the synapses are affected by DBS treatment. In order to relate the microdialysis data to their anatomical origin and to the effects of DBS, it is suitable to estimate the tissue volume which is sampled during a microdialysis experiment. In this thesis, the maximum tissue volume of influence (TVI_{max}) for a microdialysis catheter was simulated and evaluated using the finite element method (FEM), to allow interpretation of biochemical data in relation to anatomical structures.

A FEM model for simulation of the TVI_{max} for a microdialysis catheter placed in grey brain matter was set up, using Fick's law of diffusion. The model was used to investigate the impact of the analyte diffusion coefficient (D), the tissue tortuosity (λ) and the loss rate constant (k) on the size of the TVI_{max} by regression analysis. Using relevant parameter intervals, the radius of the TVI_{max} of a neurotransmitter was estimated to 0.85 ± 0.25 mm. A microdialysis experiment on calf brain tissue showed agreement with the regression model. A heterogeneous anisotropic FEM model based on diffusion tensor imaging (DTI) showed that the radius of the TVI_{max} may vary by up to 0.5 mm as a consequence of local tissue properties, which was reasonable in relation to the 95% confidence interval from the regression estimation. The TVI_{max} was simulated and patient-specifically visualized in relation to MRI images for four patients undergoing microdialysis in parallel to DBS. The size of the TVI_{max} showed to be relevant in relation to the basal ganglia nuclei, and the obtained microdialysis data indicated that the biochemical response to DBS depends on the catheter position. The simulations of the TVI_{max} were combined with patient-specific DBS electric field simulations, for further interpretation of the results in relation to the effects of DBS.

In conclusion, simulations and visualizations of the TVI_{max} allowed relating microdialysis data to its anatomical origin. Detailed knowledge about the parameters affecting the microdialysis sampling volume is valuable for the current application as well as other applications related to the migration of analytes in tissue.

Sammanfattning

Mikrodialys är en metod som används för studera lokala nivåer av biokemiska substanser i ett specifict organ eller struktur. Metoden använder sig av en kateter med ett semipermeabelt membran, över vilket utbyte av substanser sker genom diffusion. Mikrodialys har nyligen använts för att studera nivåer av neurotransmittorer i de djupa hjärnstrukturerna, ävan kallade basala ganglierna, under djup hjärnstimulering (DBS) för patienter med Parkinsons sjukdom. De basala ganglierna består av ett antal millimeterstora hjärnstrukturer, sammankopplade via biokemiska synapser, och nivåerna av signalsubstanser runt dessa synapser tros påverkas av DBS. För att relatera mikrodialysmätningarna till dess anatomiska ursprung, och till effekterna av DBS, är det önskvärt att få en uppskattning av den vävnadsvolym som påverkar mätningen från en mikrodialyskateter. Målet med denna licentiatavhandling har varit att simulera och utvärdera den maximala påverkansvolymen (TVI_{max}) för en mikrodialyskateter med hjälp av finita element-metoden (FEM), för att underlätta tolkningen av de biokemiska data som samlats in.

En FEM-modell sattes upp för att simulera TVI_{max} för en kateter placerad i grå hjärnvävnad, baserat på Ficks diffusionslag och lämpliga rand- och initialvillkor. Modellen användes för att göra en regressionsanalys av hur TVI_{max} påverkades av analytens diffusionskoefficient (D), hjärnvävnadens tortuositet (λ) och analytens nedbrytningshastighet (k), och radien för TVI_{max} för en neurotransmitter uppskattades till 0.85 ± 0.25 mm då fysiologiskt relevanta parameterintervall användes. En experimentell studie av mikrodialys på hjärnvävnad från kalv gav god överensstämmelse med simuleringsresultaten. En heterogen och anisotrop FEM-modell sattes upp med hjälp av diffusionstensordata (DTI), vilket visade att lokala vävnadsegenskaper påverkar diffusionen av analyter i de basala ganglierna med upp till 0.5 mm i enighet med den regressionsmodell som tagits fram. TVI_{max} simulerades och visualiserades sedan i relation till MRI-bilder för fyra patienter som genomgått mikrodialys parallellt med DBS. Målområdena för mikrodialysmätningarna visade sig skilja mellan patienterna, och den insamlade mikrodialysdatan indikerade att den biokemiska responsen på DBS berodde på kateterns position. För att ytterligare underlätta tolkningen av resultatet i relation till effekterna av DBS, kombinerades TVI_{max}-simuleringarna med simuleringar av det elektriska fältet runt DBS-elektroderna.

Sammanfattningsvis kan simuleringar av TVI_{max} vara en hjälp vid den fysiologiska tolkningen av insamlad mikrodialysdata, vilket underlättar jämförelser mellan patienter. Detaljerad kunskap om de parametrar som påverkar samplingsvolymen för en mikrodialyskateter är värdefulla både för den aktuella applikationen, och övriga applikationer relaterade till diffusion av substanser i vävnad.

List of Publications

The following publications, referred to by their Roman numerals, are included in this thesis:

I. Diczfalusy E, Zsigmond P, Dizdar N, Kullman A, Loyd D and Wårdell K (2011) *A model for simulation and patient-specific visualization of the tissue volume of influence during brain microdialysis,* Medical & Biological Engineering and Computing, vol 49, pp 1459–1469

II. Diczfalusy E, Dizdar N, Zsigmond P, Kullman A, Loyd D and Wårdell K *Simulations and visualizations for interpretation of brain microdialysis data during deep brain stimulation*, 34th Annual International Conference of the IEEE Engineering in Medicine and Biology Society, San Diego, USA (In Press, 2012)

III. Diczfalusy E, Andersson M, Wårdell K *The effect of tissue heterogeneity and anisotropy on microdialysis of the deep brain – a diffusion tensor based simulation study* (In Manuscript, 2012)

Related publications:

Diczfalusy E, Dizdar N, Kullman A, Åström M, Zsigmond P, Wårdell K (2010) *Biochemical monitoring and simulation of the electric field during deep brain stimulation*, XIX Congress of the European Stereotactic and functional neurosurgery (ESSFN), Athens, 22-25 September 2010.

Diczfalusy E, Åström M, Dizdar N, Kullman A, Zsigmond P, Wårdell K (2010) *A finite element model for biochemical monitoring in the brain during deep brain stimulation*, World Congress of Neurotechnology, Rome, 11-14 October 2010.

Wårdell K, Diczfalusy E, Åström M (2011) *Patient-specific modeling and simulation of deep brain stimulation*, In: Studies in Mechanobiology, Tissue Engineering and Biomaterials, Springer-Verlag, Berlin-Heidelberg, 2011.

Abbreviations

BBB	Blood-brain barrier
CN	Caudate nucleus
CSF	Cerebrospinal fluid
CT	Computed tomography
DBS	Deep brain stimulation
DTI	Diffusion tensor imaging
ECS	Extracellular space
FEM	Finite element method
GABA	Gamma-aminobutyric acid
GP	Globus pallidus
GPe	Globus pallidus externa
GPi	Globus pallidus interna
MRI	Magnetic resonance imaging
PD	Parkinson's disease
PPN	Pedunculopontine tegmental nucleus
r_{TVImax}	Radius of the maximum tissue volume of influence
SN	Substantia nigra
SNr	Substantia nigra compacta
SNr	Substantia nigra reticulata
STN	Subthalamic nucleus
TVI_{max}	Maximum tissue volume of influence

Physical symbols

Scalar symbols are written in italic, vector and tensor symbols are written in bold italic.

μ	Magnetic permeability (V·s/A·m)
C	Concentration (mol/L)
c_b	Analyte concentration at microdialysis catheter boundary (mol/L)
D	Diffusion coefficient (m^2/s)
$\boldsymbol{D}$	Diffusion tensor
Da	Dalton (Da)
D_e	Effective diffusion coefficient (m^2/s)
f	Frequency (Hz)
$\boldsymbol{J}$	Current density (A/m^2)
k	Loss rate constant (s^{-1})
M_r	Relative molecule mass (-)
Q	Analyte generation term (-)
R^2	Coefficient of determination (-)
u	Phase velocity of an electromagnetic wave (m/s)
$\boldsymbol{v}$	Bulk flow (m/s)
V	Electric potential (V)
α	Volume fraction (-)
ε	Electric permittivity (A·s/V·m)
λ	Tortuosity (-)
λ'	Wavelength of a field in tissue (m)
σ	Electric conductivity (S/m)

Table of contents

1 Introduction

Microdialysis is a method for local sampling of biochemical substances. A recent application for microdialysis is the monitoring of neurotransmitter levels in the basal ganglia in relation to deep brain stimulation (DBS). DBS is an electric stimulation technique which is widely used in clinical practice for treatment of movement disorders such as Parkinson´s disease. The mechanisms of DBS are not entirely clear, and the study of neurotransmitter levels in the basal ganglia may therefore contribute to increased knowledge about the underlying biochemical pathways. To relate the microdialysis sampling and electric stimulation to anatomical structures, patient-specific simulations and visualizations based on the finite element method (FEM) can be used. This chapter provides an introduction to the anatomical and technical aspects of microdialysis and DBS, as well as to the imaging techniques and computational methods used in this thesis.

1.1 The brain

The brain is the body´s main control and integration unit, where signals from different body parts are registered, integrated and processed. It is the centre for thoughts, emotions, behaviour and memory, all achieved through more or less complex neural processes. The brain is a differentiated organ, with a number of regions specialized for different functions. An adult brain consists of four main parts: the brainstem, the cerebellum, the diencephalon and the cerebrum (Figure 1) [1].

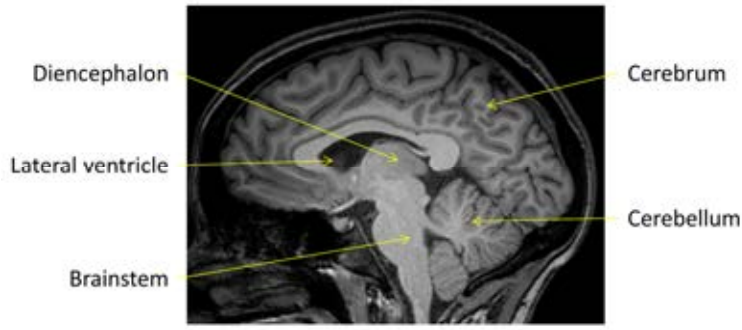

Figure 1. The main parts of the human brain, based on T1-MRI imaging.

1.1.1 Neural cells and nerve signals

The brain is mainly made up of two kinds of cells; neural cells (neurons) and neuroglia. Neurons are responsible for transmitting information within the brain and to the rest of the nervous system, allowing functions such as sensing, thinking and controlling movements. The basic parts of a neuron are the cell body, the dendrites and the axon, as shown in Figure 2a. The cell body contains the nucleus of the neuron, as well as other organelles necessary for the maintenance and function of the cell. The dendrites are the input parts of the neuron, handling incoming signals from other nerve cells, while the axon is the output part propagating nerve impulses towards the synaptic cleft and further to the surrounding cells [2]. Many axons are covered by a protecting and insulating layer known as myelin, in order to insulate and increase the speed of the propagating nerve signals. The myelin is provided by neuroglia cells known as Schwann cells and oligodendrocytes. Overall, neuroglia cells have a supporting function, providing both mechanical and chemical protection to the neurons. The name originates from the fact that neuroglia were originally considered as glue that held the nervous system together [1].

Neurons have a resting membrane potential of about -70 mV, due to a small build-up of negative ions in the cytosol of the cell and a build-up of positive charges in the surrounding extracellular fluid. Numerous ion channels exist in the cell membrane, and when some of these channels open – usually triggered by stimuli such as chemical ligands, mechanical disruption or voltage changes – the membrane potential changes. When a threshold value of about -55 mV is reached, a nerve impulse (action potential) is triggered, propagating the nerve signal throughout the axon. Each nerve impulse consists of a depolarizing phase, caused by an opening of sodium channels, a repolarizing phase, during which potassium channels open, and an after-hypopolarization phase after which the resting state of the membrane is restored [1, 2].

Nerve signals are transmitted from one cell to the next through the synapse (Figure 2b), which is a physical space in between neurons. The synapse may be either electric or chemical; chemical synapses are much more common within the brain [3]. The chemical synapse consists of a synaptic cleft, a fluid-filled space of 20-50 nm [1], between the presynaptic and postsynaptic neurons. In response to a nerve impulse in the presynaptic neuron, certain chemicals, known as neurotransmitters, are released into the synaptic cleft. The

neurotransmitters diffuse through the synaptic fluid and binds to receptors in the membrane of the postsynaptic cell, thereby initiating a postsynaptic potential. The postsynaptic potential may be a depolarization or hyperpolarization, depending on the nature of the neurotransmitter and the receptor. Neurotransmitters causing a depolarizing postsynaptic potential are called excitatory, while neurotransmitters that hyperpolarize the membrane are called inhibitory. Once released, the neurotransmitters which do not bind to a receptor will be quickly removed from the synaptic cleft by either diffusion out of the synaptic cleft, enzymatic degradation or re-uptake of the substance into the cell [3, 4].

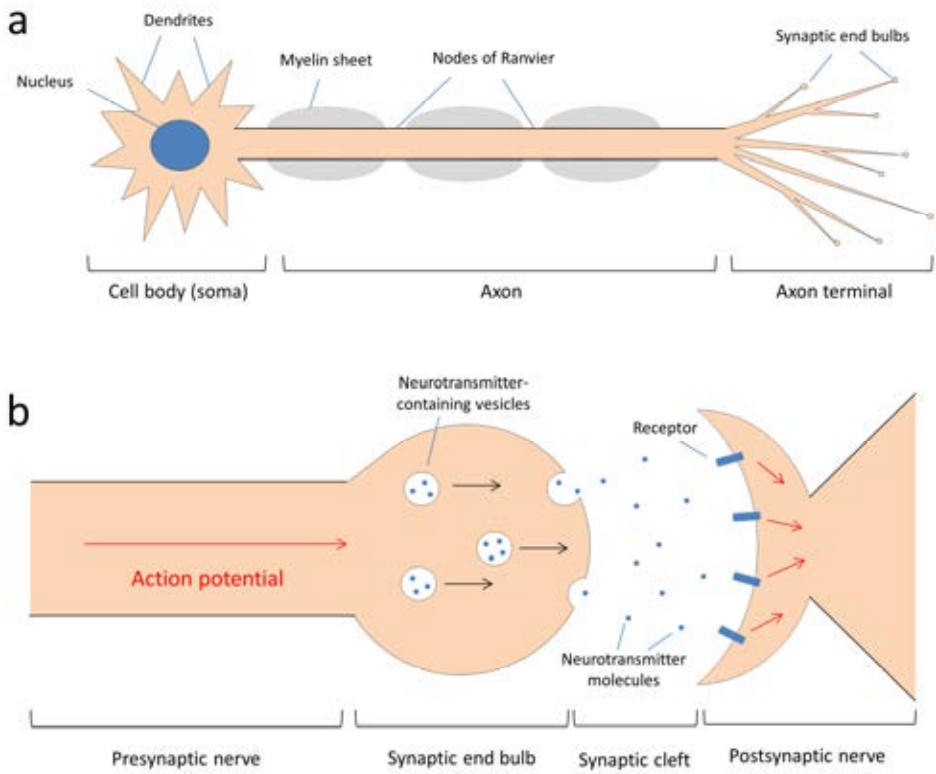

Figure 2. a) The basic parts of a neuron **b)** Neural signal transmission through the synapse

1.1.2 Tissues of the brain

On a tissue level, the brain consists of grey matter, white matter, blood and cerebrospinal fluid (CSF). Grey matter contains neuronal cell bodies, dendrites, unmyelinated axons and neuroglia. Specific organelles of the neuronal cell body, known as Nissl bodies, give grey matter its greyish look. Grey matter makes up the outer rim of the brain, known as the cortex, as well as several cell body clusterings inside the brain called nuclei. White matter contains myelinated axons, and appears white due to the myelin provided by the neuroglia cells. White matter makes up fibre tracts, which are distributed throughout the brain in order to transmit signals to and from the cortex and the grey nuclei. CSF is a clear liquid which circulates around the brain and the spinal cord, as well as in cavities within them. There are four CSF-filled cavities within the brain known as the ventricles; there are two lateral ventricles located within each hemisphere of the cerebellum (as illustrated in Figure 1), a third ventricle located between the right and left halves of the thalamus, and the fourth ventricle which lies between the cerebellum and the brain stem. The CSF is formed in capillaries in the walls of the lateral ventricles and the roof of the third ventricle, flows towards the fourth ventricle, and on to the subarachonid space which surrounds the brain and spinal cord. The subarachnoid space contains finger-like structures called arachnoid villi, where the CSF is reabsorbed into the blood [4, 5]. The CSF circulation provides mechanical and chemical protection to the brain, and allows substance exchange between the brain and the blood in order to provide the brain with nutrients and remove waste products [4].

Blood vessels are present in both white and grey matter, with blood entering the brain mainly from vertebral arteries and arteries on the sides of the head and neck called the internal carotid. Grey matter is more vascularized than white matter, because of its higher cell content resulting in higher oxygen consumption. Brain capillaries are lined with endothelial cells, but lack the micropore system which is characteristic for capillaries in other parts of the circulation. Therefore, the walls of the brain capillaries are referred to as the blood-brain barrier (BBB). The BBB has a very low permeability for most molecules, thereby protecting the brain from harmful substances. Only small, lipid-soluble substances such as oxygen and carbon dioxide are allowed to diffuse freely over the BBB, while the transport of other substances require active transport mechanisms [5].

1.1.3 The basal ganglia

The basal ganglia are a group of interconnected grey nuclei embedded within the cerebral hemispheres. These nuclei have important roles in the initiation, regulation and termination of body movements, and are also involved in cognitive, limbic and linguistic functions [1, 6]. The pathophysiology of common movement disorders such as Parkinson´s and Huntington´s diseases are related to basal ganglia dysfunction [6]. The correct term would be the basal nuclei, since ganglia usually refers to groups of cell bodies outside of the brain [7]; the basal ganglia is, however, the term commonly used in neuroscience and will therefore be used throughout this thesis.

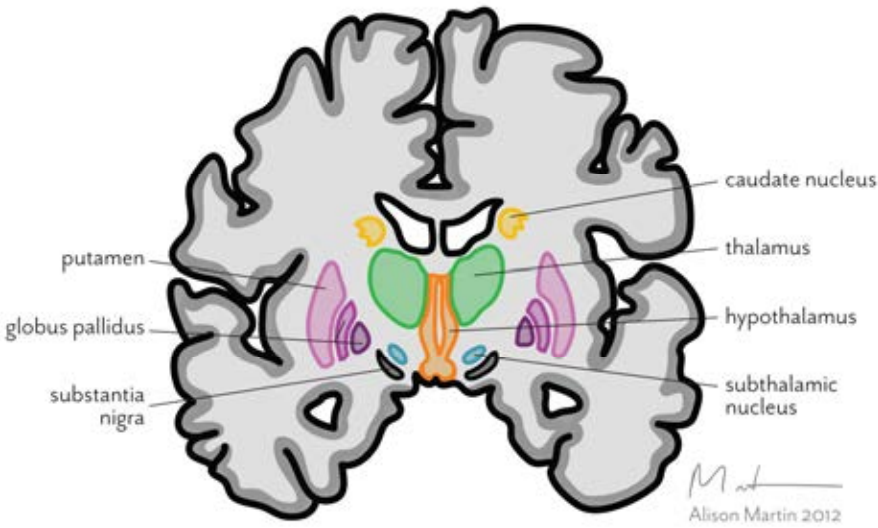

Figure 3. Schematic illustration of the basal ganglia nuclei, here shown in a coronal slice of the brain. Courtesy of Alison Martin (www.sketchymedicine.com)

Although the definition of the basal ganglia varies in the literature, three interconnected nuclei are generally considered to be its main components: the caudate nucleus (CN), the putamen and the globus pallidus (GP). The GP is divided into an internal part (globus pallidus interna, GPi) and an external part (globus pallidus externa, GPe), separated by a thin white lamina. The CN and the putamen are together commonly referred to as the striatum, which is often regarded as the main input station for afferent signals to the basal ganglia network from other parts of the brain. Three additional nuclei, namely the subthalamic nucleus (STN), the substantia nigra (SN) and the pedunculopontine tegmental nucleus (PPN) are integral parts of the pathways through the basal ganglia, although they are not formally parts of it [7, 8]. The

basal ganglia network is connected to the cortex and the thalamus, a nuclei positioned within the diencephalon which helps transmit sensory and motor signals between the different parts of the brain [1].

An overview of the basal ganglia and the surrounding structures is shown in Figure 3. As illustrated in Figure 4, the neural pathways of the basal ganglia are either excitatory or inhibitory, depending on the neurotransmitters that are involved in the synaptic signal transmission. Common neurotransmitters of the basal ganglia include acetylcholine and glutamate which are excitatory, gamma aminobutyric acid (GABA) which is inhibitory, and dopamine and serotonin which may be both inhibitory and excitatory depending on the type of receptor they bind to [1, 9]. The basal ganglia network has been modelled both as a hierarchical network and as a more complex, parallel-acting system of positive and negative feedback systems that "sum up" in the cortex [10-12]. The striatum receives neural input from the cortex, the thalamus and the substantia nigra compacta (SNc). Neural signals are then transmitted from the striatum through the basal ganglia network, projecting to the thalamus and then back to the cortex [12]. The signals through the basal ganglia are thought to be transmitted mainly by two neural paths, called the direct and indirect pathways (Figure 4).

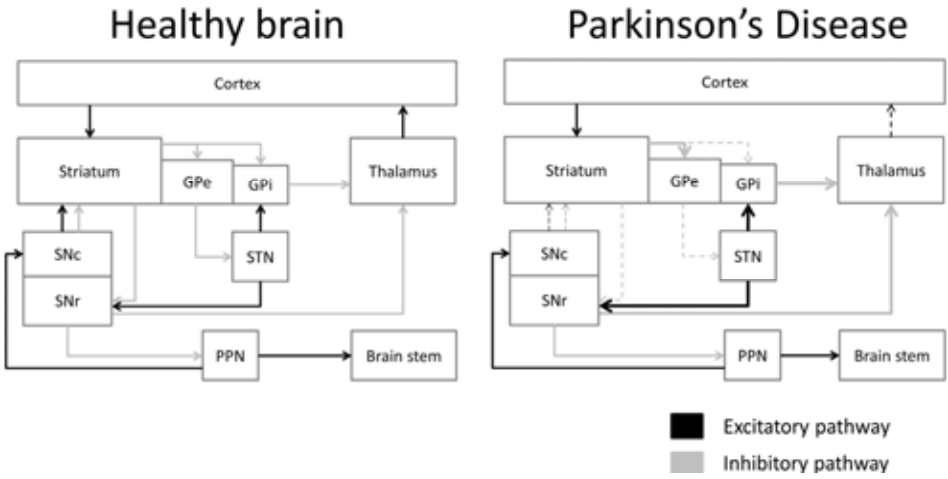

Figure 4. The main neural pathways of the basal ganglia network, based on [7, 8]. Excitatory pathways are shown in black, inhibitory pathways in grey. The left image shows the pathways of a healthy brain, while the right image shows the imbalance caused by Parkinson's disease. The neural pathways from the SNc to the striatum are here degenerated, as indicated by thin dashed arrows.

The direct pathway goes from the striatum, projects to the internal globus pallidus (GPi) and the substantia nigra reticulata (SNr) which in turn provides output to the thalamus. In the indirect path, signals are projected through the striatum, to the external globus pallidus (GPe), further on to the STN and then to the GPi and the SNr. The direct and indirect pathways are thought to have opposite effects on the GPi/SNr projections, and the balance between the activities of the pathways regulates the cortical output [7].

1.1.4 Parkinson´s disease

Parkinson´s disease (PD) is one of the world´s most common neurodegenerative disorders, affecting more than 4 millions of people worldwide [13]. The cardinal features of PD relate to motor dysfunctions, including tremor, dystonia, akinesia and postural instability, but the disease may also include psychiatric symptoms such as anxiety, apathy and depression [14]. PD is thought to stem from a combination of environmental and genetic factors, and is difficult to diagnose due to a lack of biomarkers or visible neuroimaging findings. Therefore, PD is diagnosed based on clinical criteria; mainly the presence of parkinsonian symptoms which cannot be related to other causes [15].

Pathologically, PD is mainly characterized by degeneration of dopaminergic neurons extending from the SNc to the striatum. This degeneration causes an imbalance of neurotransmitter substances in the basal ganglia, affecting dopaminergic as well as non-dopaminergic transmission systems [9]. A summary of how the dopamine depletion affects the pathways of the basal ganglia is seen in Figure 4. Currently, there is no known cure for PD; levodopa medication, which acts as dopamine therapy, is commonly used for symptom relief [16, 17]. As the disorder progresses, symptoms may worsen and side disorders may occur as a consequence of increased medication. In such cases, surgical procedures such as radiofrequency lesioning and deep brain stimulation (DBS) can be used as complementary therapies [17].

1.2 Deep brain stimulation (DBS)

DBS is a technique for electric stimulation of deep brain structures, within or surrounding the basal ganglia. During the last decades, more than 40 000 patients over the world have received DBS implants, showing marked improvements for a growing number of movement disorders [18-20]. The most common DBS application areas include PD, essential tremor and

dystonia. DBS has been approved for PD and essential tremor in the US, Canada, Europe and Australia, and for dystonia in the US [21]. With a high variability and reversibility, DBS offers important advantages over therapies such as radiofrequency lesioning and pharmacological treatment [19]. Besides movement disorders, DBS is also being explored as a treatment option for neuropsychiatric disorders such as depression, obsessive-compulsive disorder and Tourette´s syndrome [21].

1.2.1 Principles of DBS

In DBS, continuous electrical stimulation is delivered to a pre-defined target area within the brain through chronically implanted electrodes (Figure 5), usually containing multiple contacts [22]. Common target sites for treatment of movement disorders are the STN, the GPi and the ventralis intermediate nucleus (Vim) of the thalamus [21]. The electrodes are connected to an electric stimulator, through which the amplitude of the delivered voltage or current, the pulse width and the frequency can be regulated. By targeting different areas within the brain and by varying stimulation parameters and which electrode contacts to use, DBS can be well adapted depending on the patient´s needs [10]. Commercially available DBS electrodes are about 1.3 mm in diameter, with typical DBS settings ranging from 1-5 V for electric potential, 60-200 μs for pulse width and 130-180 Hz for frequency [23].

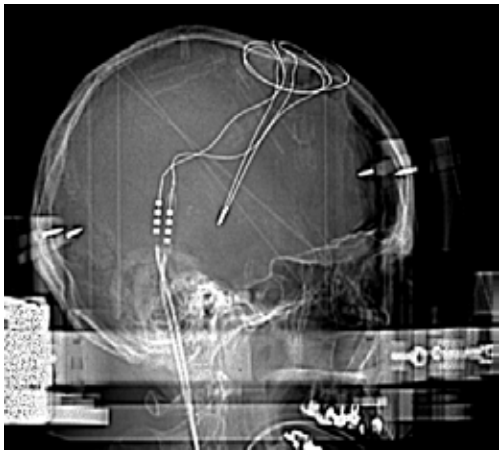

Figure 5. X-ray image showing DBS electrodes bilaterally implanted in the subthalamic nucleus (STN).

The insertion of DBS electrodes is performed using stereotactic surgery, based on pre-operative imaging and planning (Figure 6) [10]. The stereotactic procedure begins by placing a stereotactic frame on the head of the patient. An indicator box is then applied to the frame, in order to provide fiducials to act as a reference system in the images, and anatomical imaging of the patient´s head is performed. Magnetic resonance imaging (MRI) or computed tomography (CT) is used to obtain the images; commonly, MRI is performed a few days before the implantation, and is then fused with a stereotactic CT obtained on the day of surgery [20]. The pre-operative images are used to identify a suitable entry point and a trajectory towards the DBS target area, where blood vessels and other sensitive structures are avoided. The target can be localized either by direct targeting, based on the pre-operative images, or indirect targeting, based on stereotactic atlases and well-defined brain landmarks [22]. The calculation of coordinates for the intervention is usually performed using commercially available stereotactic software, such as SurgiPlan (Elekta Instrument AB, Stockholm, Sweden), iPlan (BrainLab AG, Munich, Germany), Framelink (Medtronic Incorporation, Minneapolis, MN, USA) or STP (Stereotactic Treatment Planning System; Howmedica Leibinger GmbH, Freiburg, Germany) [20].

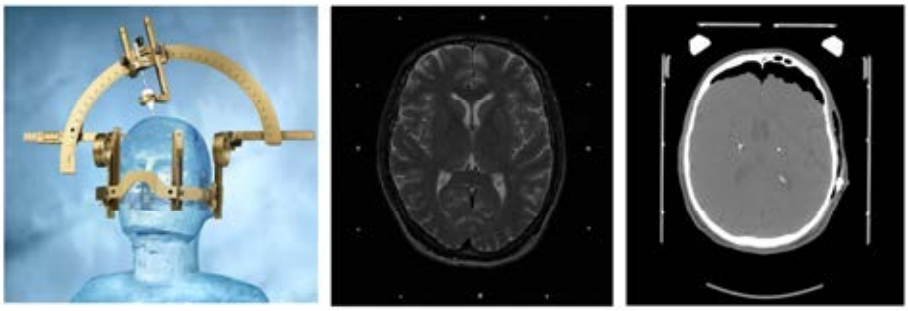

Figure 6. Stereotactic implantation of DBS electrodes. A stereotactic frame is placed on the head of the patient, and a stereotactic arc is used for the electrode insertion, as seen in the left image (Courtesy of Elekta Instrument AB, Sweden). The middle image shows a preoperative MRI image with stereotactic reference coordinates, seen as bright spots. The right image shows a postoperative stereotactic CT, where the inserted DBS electrodes are visible as bright artefacts.

For electrode implantation, a stereotactic arc is attached to the head frame to precisely locate the entry point where a burr hole is made [22]. Intraoperative measurements such as microelectrode recording [24], impedance recording [25] and optical methods [26] can be used prior to electrode insertion, to help confirm that the desired target area has been reached.

If the patient is awake during the intervention, DBS electrodes can be tested for efficacy and side effects before the electrode is anchored and secured in place. Finally, the pulse generator is connected to the electrode lead and implanted in the clavicular area. This may be performed immediately after surgery, or several days later [22]. Post-operative MRI or CT imaging (Figure 6) is usually performed in order to verify that the intended target area has been reached [20].

1.2.2 Advantages, disadvantages and limitations

The greatest benefits of DBS are the reversibility of its effect and the ability to adjust stimulation parameters depending on the target area, the condition to be treated and the patient´s needs [10]. The main disadvantages include the invasiveness of the technique, associated with an increased risk of intracranial bleeding and infections, and potential side effects if the electrodes are incorrectly inserted [18]. Hardware-related complications such as electrode breakage, electrode migration and skin erosions around the pulse generator have also been reported [27].

1.3 Microdialysis

Microdialysis is an invasive method used for monitoring of the local biochemical environment in a region of interest. The technique uses a catheter with a semi-permeable membrane, allowing measurements of practically all substances smaller than the membrane pores as long as a suitable detection technique is available. Microdialysis of the brain, also known as cerebral microdialysis, is today the most common method for sampling neurochemicals in deep brain structures in vivo for clinical research purposes [28].

Cerebral microdialysis is well established as a laboratory tool, and is also being increasingly used for bedside monitoring during neurointensive care [29, 30]. Clinical microdialysis research applications include conditions such as traumatic brain injury, subarachnoid haemorrhage, ischemic stroke, epilepsy and movement disorders. Within the field of movement disorders, microdialysis has been used in parallel to DBS for patients with PD, to study the local neurochemical environment in basal ganglia structures associated with movement [31-34]. Substances commonly sampled by cerebral microdialysis include dopamine, GABA, glutamate, nitric oxide, glucose, lactate and pyruvate [28].

1.3.1 Principles of microdialysis

The basic principle of microdialysis (Figure 7) is to mimic the passive function of a blood capillary. The microdialysis catheter consists of an inner tube, usually ranging from 0.1-0.3 mm in diameter, and an outer semipermeable membrane. The catheter is continuously perfused with a saline solution, called the perfusate. Substance exchange will occur over the membrane, using the concentration gradient between the perfusate and the surrounding medium as the main driving force. Following the substance exchange over the membrane, the resulting microdialysis sample (termed dialysate) is transported through an outlet and collected for analysis [35-37].

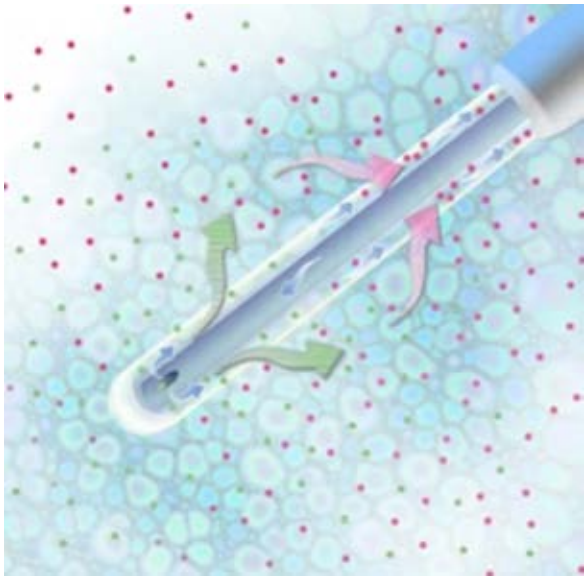

Figure 7. The principle of microdialysis. Perfusate fluid passes through the catheter, and substance exchange occurs over the membrane depending on the chemical composition of the perfusate and surrounding medium. The perfusate may flow either from the inner tube and out, as illustrated here, or in the opposite direction, depending on the composition of the catheter. Courtesy of CMA Microdialysis AB, Sweden.

The content of the dialysate depends on the pore size (cut-off) of the catheter membrane. Small pore sizes (≤ 20 kDa) allow collection of small molecules such as neurotransmitters, while pore sizes up to 100 kDa are used to collect macromolecules such as proteins [38]. The relation between the concentration of an analyte in the dialysate and the actual analyte concentration of the surrounding extracellular space is called relative recovery, and depends on parameters such as membrane geometry, flow rate, molecular weight, temperature, and

sample tortuosity. When performing quantitative microdialysis, knowledge of the extraction fraction is crucial in order to draw conclusions about the actual substance concentration in the tissue [39]. When studying the pattern of concentration change of a substance over time, e.g. in response to a stimulus, the extraction fraction is of less importance.

When sampling small targets such as deep brain nuclei, which are in the millimeter range, the size of the microdialysis catheter is critical in order to to restrict sampling to only the desired area. Furthermore, the exact placement of the microdialysis catheter must be carefully evaluated and confirmed, especially if the data is meant to reflect the physiology of a particular structure. This confirmation is facilitated by the fact that some commercially available catheters contain a marker at the tip, allowing confirmation of placement by CT or X-ray scan [28, 29]. For brain microdialysis, it should be kept in mind that microdialysis catheters do not sample neurochemicals directly at their release site (such as in the synaptic cleft); instead, it detects the compound in the extracellular fluid surrounding the catheter [40].

1.3.2 Advantages, disadvantages and limitations

Since microdialysis is an invasive technique, there is a considerable risk of tissue injury [39]. Therefore, cerebral microdialysis is usually applied only when intervention of the brain is already being performed for other reasons. There are few reports of significant injuries from microdialysis in the literature, however [28]. A clear limitation of the technique is the limited time resolution; mean values for a defined period are provided rather than real-time data [39]. The local sampling of a microdialysis catheter is usually considered an advantage, when sampling from a specific structure is desired, but this may also be a limitation if a larger structure or the whole brain is to be studied [28].

1.4 Brain imaging techniques

1.4.1 Magnetic resonance imaging (MRI)

MRI is an imaging technique which has been used commercially since the 1980's [41]. MRI provides a better soft tissue contrast than tissue density based imaging techniques, such as computed tomography (CT), and is also considered safer since it does not involve any ionizing radiation. MRI has therefore gained enormous popularity within clinical imaging and research, and is today considered an essential tool for the diagnosis of brain and nervous

system related disorders. It is also being increasingly used for other body parts such as the heart and the liver [41, 42].

In MRI, the positively charged proton of the hydrogen nuclei is being imaged. A proton has a specific minute magnetic field depending on its charge and spin. When a magnetic field is applied the protons will align with respect to the field. When a radio frequency pulse is applied at the Larmor, or resonance, frequency (42.6 MHz/T), the protons will absorb the energy and start to precess around the main axis of the magnetic field.

While releasing the absorbed energy and returning to the original, "relaxed" state the protons will act as small radio transmitters. There is no way to distinguish the signal from each proton but the joint signal of all excited protons is recorded over time. Now by applying small gradients to the magnetic field during the relaxation the Larmor frequency of the protons now acting as radio transmitters will vary over position and time, q. This feature provides the means to estimate the spatial distribution of the protons but not in terms of a conventional image. These so called k-space samples correspond to the Fourier domain and the spatial image is accessed via an inverse Fourier transform.

The relaxation time for a proton can be described as T1 (spin-lattice relaxation) or T2 (spin-spin relaxation). In the relaxation process, the protons will produce a voltage which is recorded by the MRI scanner, thereby providing information for the resulting intensity image [41]. A MRI image can be T1-weighted, T2-weighted or proton density (spin-density) weighted. The final image intensities depends on parameters such as magnetic field strength, pulse sequence and tissue characteristics. Generally, tissues with a high content of free water (such as CSF) appear dark in T1-weighted images and bright in T2- and proton density-weighted images. Different types of MRI images are used clinically depending on the tissue and the disease to be diagnosed [20, 42]; within the area of stereotactic surgery, proton density is preferred for visualization of the GP, while T2 offers a better view of the STN [20]. Examples of T1, T2 and proton density MRI images are shown in Figure 8.

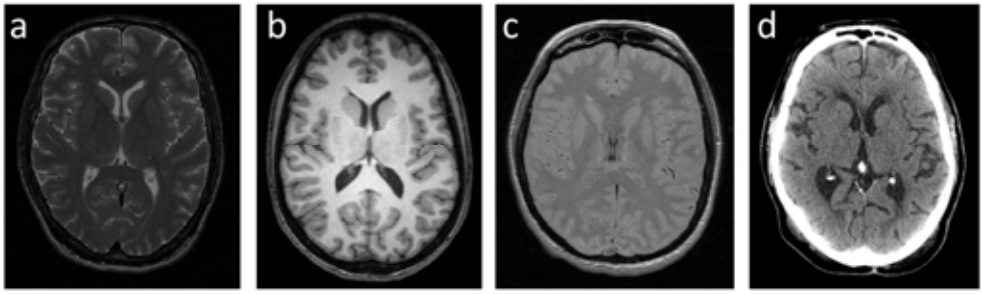

Figure 8. MRI and CT images of the brain. **a)** T2-weighted MRI **b)** T1-weighted MRI **c)** Proton density weighted MRI (Courtesy of Unit of Functional Neurosurgery, Queen Square , London) **d)** CT.

1.4.2 Diffusion tensor imaging (DTI)

DTI is an MRI-based imaging method which aims to describe the three-dimensional diffusion of water molecules within the brain. DTI stems from "plain" diffusion MRI, which is a method for describing the overall diffusivity of water in brain tissue. Diffusion MRI images are obtained by making the MRI signals sensitive to the diffusion process, using a pair of sharp magnetic field gradient pulses. The first pulse is said to "label" each hydrogen nuclei according to its spatial location, the second pulse is introduced shortly after to detect the displacement that occurred between the pulses (this time interval is known as the diffusion time) [43]. A diffusion MRI image shows the statistical displacement distribution of water molecules within each voxel, presented as a scalar value. DTI images are obtained by collecting diffusion MRI images along several gradient directions, thereby allowing the determination of a second-order tensor model to describe the water diffusion [44].

Diffusion is a physical process that is completely independent of the magnetic field from the MRI scanner, so the imaging does not interfere with the natural diffusion occurring in the tissue. DTI is a powerful tool for exploring the local tissue structure, and is used in clinical research for applications such as white matter tracing [45, 46], detection of brain ischemia [44] and prediction of drug delivery to the brain [47, 48]. It has also been suggested that DTI data is directly related to the electric conductivity of brain tissue [49], and DTI images have therefore been used to simulate the electric potential distribution in the brain during DBS [50-52].

1.4.3 Computed tomography (CT)

CT was introduced clinically in 1972, and was the first conventionally used radiological imaging technique that provided computed, digital images. In CT, an X-ray radiation source is rotated around an axis, producing beams with an intensity which is recorded by a detector on the opposite side of the rotation axis. The intensity is measured either in single points or continuously, resulting in an intensity profile. By using inverse transformation, the resulting image can be extracted from the intensity profile. The CT intensities corresponding to different materials for a specific scan are determined depending on their density or attenuation value in relation to water, which are expressed in Hounsfield units (HU) [53]. An example of a brain CT image is included in Figure 8, where bone, having a high HU, appears bright in relation to the soft tissues of the brain.

Clinically, CT is widely used for organs such as the lung, breast, stomach and brain, although criticized for involving large radiation doses [54]. For applications such as DBS implantation, where the exact anatomy of the brain is crucial, CT and MRI are often merged in order to provide a detailed representation of the brain. MRI is considered superior for visualization of soft tissue structures, while CT is is less susceptible to distortions from magnetic field inhomogeneities [20, 22].

1.5 The finite element method

The finite element method (FEM) is a numerical method used to find approximate solutions to the distribution of field variables within a defined system [55]. The method was originally developed for static structural analysis, but has later been extended to cover domains such as fluid flow analysis, thermal analysis and electric analysis. In recent years, with an increasing understanding of medical and biological systems, FEM has gained popularity for biomedical applications [56]. Topics such as electric field distributions in the brain [57-59], hemodynamics [60, 61], intracranial drug delivery [48, 62], and brain lesioning [63, 64] have all been explored using FEM models.

1.5.1 Overview of a FEM simulation

The first step of any FEM simulation is the definition of the system to be analysed; the exact geometry, the material properties or environmental effects and the boundary conditions are all included in this concept. The next step is the discretization, where the system is divided into a

finite number of elements which are connected to each other by nodes located at the element edges or corners. The elements may have different shapes, such as triangular, quadratic or cubic (Figure 9). Elements with straight sides are called linear elements, while elements with curved edges are called higher-order elements and are modelled by introducing midpoint nodes [65].

At each node, the physical quantities of interest are identified, and element equations, also called governing equations, for all elements in the domain are generated. The generation of element equations include determination of the displacement function, which interpolates the displacement field within an element based on the node values. The generated element equations are then assembled to produce the total system equation, based on nodal equilibrium. The boundary conditions, defined in the first step, are then introduced into the system equation [55].

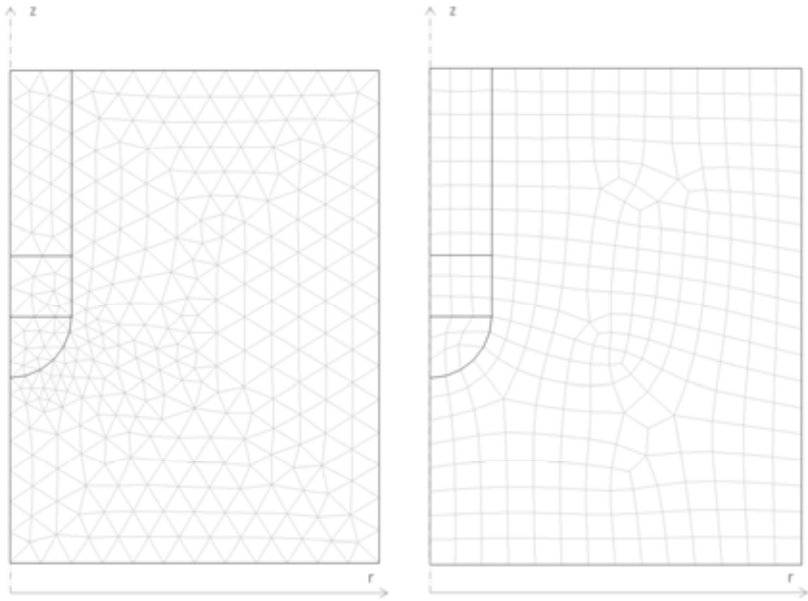

Figure 9. Two examples of meshing (discretization) of a two-dimensional FEM model of a brain electrode. The meshes shown here are have been automatically generated by the FEM software (COMSOL Multiphysics 3.5, Comsol AB, Stockholm, Sweden) with the largest number of elements around corners and edges close to the active electrode. **a)** Triangular mesh elements **b)** Quadratic mesh elements.

Once the complete system equation has been set up, suitable mathematical methods for solving simultaneous equations are used to find the unknown values, or displacements, at the nodes. Direct or iterative mathematical methods can be used; direct methods are generally considered faster and are suitable for small systems, while iterative methods produce less round-off errors and are preferred for large systems. When the system has been solved, relevant field values can be obtained. Such field values are related to the the physical quantities which have been included in the generation of the system equation; the electric field may be obtained from an electric analysis problem, the heat flux from a heat transfer problem, and so on [55, 66].

1.5.2 Advantages, disadvantages and limitations

The strength of FEM lies in its ability to estimate field quantities for complex shapes and systems, for which analytical solutions are often unavailable. The accuracy of the method depends on the approximations and assumptions which are made about the system; an increased number of elements and associated nodes will increase the accuracy of the solution, but will yield a larger number of equations to solve. For complex problems, the number of nodal equations can easily reach hundreds of thousands or more. The method is therefore heavily dependent on computer power, and there is a number of commercial software packages available for finite element analysis [66].

2 Aim of thesis

The overall aim of the thesis was to set up patient-specific models, simulations and visualizations, in order to improve the interpretation of brain microdialysis data in relation to DBS of the STN. Specific aims were to:

- Develop a model for prediction and simulation of the tissue volume of influence (TVI_{max}) for a microdialysis catheter, using the finite element method (FEM).
- Investigate the impact of tissue- and substance-related parameters such as tortuosity, diffusion coefficient and loss rate constant on the defined TVI_{max}.
- Investigate the effect of tissue heterogeneity and anisotropy on the defined TVI_{max}.
- Set up a multiphysics model, in order to simulate and visualize both the TVI_{max} for each microdialysis catheter and the electric field extension around each DBS electrode for patients undergoing microdialysis in parallel to DBS.

3 Materials and methods

3.1 Clinical data

3.1.1 Human subjects

In Paper I and Paper II, data from four patients with Parkinson's disease (aged 56 ± 8) referred for bilateral implantation of DBS electrodes in the STN was used. The patients gave informed written consent for participation in the study (Ethically approved by the Regional Ethics Committee at Linköping University, No. 51-04). In Paper III, images obtained from the author (ED) were used.

3.1.2 Equipment and clinical procedure

The microdialysis catheters used in the study were model CMA65 (CMA Microdialysis AB, Sweden), with a membrane length of 10 mm, a diameter of 0.4 mm and a molecular cut-off at 20 kDa (Figure 10a). The DBS electrodes were Medtronics Model 3389 (Medtronics Inc. USA), which has a diameter of 1.27 mm and contains 4 evenly spaced platinum/iridium contacts. The contacts are 1.5 mm in length, and are separated by 0.5 mm (Figure 10b).

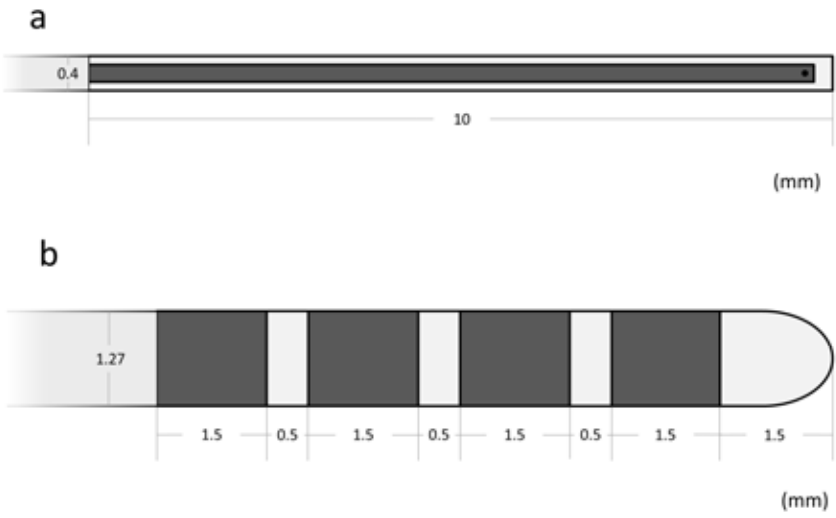

Figure 10. Geometrical dimensions of the microdialysis catheters and DBS electrodes used in this thesis. **a)** CMA65 **b)** Medtronics 3389.

The patients included in Paper I and Paper II each underwent stereotactic implantation of two DBS electrodes in the STN, and three microdialysis catheters in the putamen (right side) and the GPi (left and right side). Stereotactic imaging with a 1.5 T scanner (Achieva, Philips Healthcare, The Netherlands) was performed after placement of the Leksell® Stereotactic System (model G, Elekta Instrument AB, Sweden). Adjacent trans-axial slices of 2 mm thickness with T1 and T2-weighted sequences were used for direct anatomical targeting [67, 68]. The stereotactic images were exported to Leksell® Surgiplan (Elekta Instrument AB, Sweden) for calculation of targets and trajectories. At surgery four burr-holes were placed according to the co-ordinates of the targets. Fluoroscopy images were captured during insertion of the DBS electrodes in order to visualize the electrode positions in relation to the frame and the target coordinates. A stereotactic CT (GE Lightspeed Ultra, GE Healthcare, UK) was done directly after the implantations, to verify the electrode and catheter positions. Following imaging, each patient was referred to the neuro-intensive care unit where collection of biochemical samples was initiated. Microdialysis data was collected for 72 hours for each patient, after which the catheters were removed.

3.1.3 Image data

For the patients in Paper I and Paper II, the stereotactic preoperative T2-weighted MRI images and postoperative stereotactic CT images (Section 3.1.2) were used for modeling and visualization of brain tissue in the FEM software. For Paper III, T1-weighted MRI images and DTI images were used, obtained with a 3 T MRI scanner (Ingenia, Philips Healthcare, The Netherlands). All image details are summarized in Table 1.

Table 1. Overview of the patient image data used for the different studies.

Paper	**I - II**	**I - II**	**III**	**III**
Image type	**T2-MRI**	**CT**	**T1-MRI**	**DTI**
Field strength (T)	1.5	-	3	3
Echo time (ms)	20	-	3.6	104.7
Repetition time (ms)	8000	-	8.5	8935
Number of averages	3	-	1	2
Pixel spacing (mm)	0.98 x 0.98	0.55 x 0.55	0.75 x 0.75	1.75 x 1.75
Slice thickness (mm)	2	0.5	0.8	2

3.2 Physics

3.2.1 Diffusion of substances in brain tissue

On a macroscopic level, diffusion of a substance in a medium can be described by Fick´s second law of diffusion (Equation 1):

$$\frac{\partial C}{\partial t} = \nabla \cdot (D \nabla C) \tag{1}$$

C (mol/L) is here the substance concentration $C(x,y,z,t)$, where t is the time (s) and x,y,z (m) are space coordinates. D (m^2/s) is a parameter known as the substance diffusion coefficient. The diffusion coefficient describes the ability of an analyte to move through a medium, and depends on the physical properties of the analyte and the solvent. Values of D for different substances can be found experimentally or estimated using a suitable formula [69, 70].

Diffusion in brain tissue takes place mainly in the narrow spaces between the cells, collectively referred to as the extracellular space (ECS). The ECS contains a fluid commonly known as the interstitial fluid, and acts like a porous medium for substances which do not cross the cell membranes. Substances such as neurotransmitters transmit information to surrounding cells by moving through the ECS, a type of communication known as volume transmission [71, 72]. In order to describe the diffusion in the ECS, Equation 1 must be modified in order to take tissue-related parameters into account. Nicholson and Phillips [73] showed that an unchanged form of the equation could be used to satisfactorily quantify diffusion in the ECS, if averaged variables were used to describe the macroscopic properties of brain tissue. More specifically, two parameters were used in order to set up a volume averaged version of the diffusion equation: the volume fraction α and the tortuosity λ. Additional parameters were then introduced to account for the release and breakdown of substances as well as bulk flow within the ECS, resulting in Equation 2.

$$\frac{\partial C}{\partial t} = \nabla \cdot \left(\frac{D}{\lambda^2} \nabla C \right) + \frac{Q}{\alpha} - \boldsymbol{v} \cdot \nabla C - \frac{f(C)}{\alpha} \tag{2}$$

The tortuosity λ describes the hindrance of diffusion in brain tissue compared to a free medium, originating from factors such as geometric obstacles and nonspecific interactions

with the surrounding cell structures. It is generally assumed that the mean value of λ is about 1.6 for brain tissue, slowing down the diffusion two to three times compared to a free medium. The term D/λ^2 is often denoted $\boldsymbol{D_e}$, representing the effective diffusivity of a substance in tissue. $\boldsymbol{D_e}$ is a second-order tensor for anisotropic tissue, and can be reduced to a scalar, $D_e = \mathrm{tr}(\boldsymbol{D_e})/3$, if the tissue is isotropic [72]. The volume fraction α describes the volume of ECS in relation to the volume of the whole brain. This parameter ranges between 0.15 and 0.30, with a typical value of 0.20. Q/α is a source term representing the release of molecules into the tissue, where Q is a function of space and time, $Q(x,y,z,t)$. The source term may be excluded if the diffusion is driven by substances applied to a surface of the brain; in that case, the substance release can be accounted for through boundary conditions [71]. The term $\boldsymbol{v} \cdot \nabla C$ accounts for bulk flow, where $\boldsymbol{v}$ is a velocity vector and the velocities are functions of space and time. The existence and amount of bulk flow in brain tissue is debateable, and it is hypothesized that the bulk flow is restricted to the perivascular spaces rather than the entire ECS [74]. $f(C)/\alpha$ describes the rate of analyte loss from the ECS due to factors such as uptake into cells, transport through the blood-brain barrier or enzymatic degradation. The analyte loss is often considered to be proportional to local concentration, so that $f(C) = k\alpha C$ where k is a loss rate constant (s^{-1}) [71, 72].

In order to assure that the local medium properties are averaged, Equation 2 should only be applied to diffusion measurements with distances exceeding 100 μm [75]. When using the equation to solve a diffusion problem, it must be combined with suitable assumptions, initial conditions and boundary conditions.

3.2.2 Electric currents in tissue

The electric properties of tissues determine the pathways of current flow through the body, and are therefore of great importance for biomedical applications. Since tissue is highly heterogeneous on a microscopic level, containing a variety of cell shapes, cell distributions and extracellular properties which are difficult to mimic in detail, a macroscopic approach is usually adopted [76]. On a macroscopic level, a material is described as having electric permittivity, ε (A·s/V·m), and conductivity, σ (S/m). The permittivity describes the ability of the material to store charge, while the conductivity describes the ability to conduct electric currents. Tissue contains numerous insulating cell membranes, which work effectively as capacitors when low-frequency current is applied to the tissue. Therefore, the tissue

conductivity is low for low-frequency current and increases with higher frequencies, while the opposite is true for the permittivity [77].

In an electromagnetic sense, the wavelength (m) of a field in a medium is defined as [78]:

$$\lambda' = \frac{u}{f} = \frac{1}{f\sqrt{\varepsilon\mu}} \tag{3}$$

Here u is the phase velocity of an electromagnetic wave (m/s), μ is the magnetic permeability of the material (V·s/A·m) and f is the frequency (Hz). For typical DBS frequencies of 130-180 Hz, the value of ε is generally less than $1 \cdot 10^{-5}$ A·s/V·m [79], giving wavelengths above the meter range. When the wavelength of the applied field is much larger than the region of interest, an electrostatic approximation can be used to describe the electric potential distribution, and the equation of continuity for steady currents can be used [78, 80]:

$$\nabla \cdot \boldsymbol{J} = -\nabla \cdot [\sigma \nabla V] = 0 \tag{4}$$

$\boldsymbol{J}$ is the current density (A/m^2) and V is the electric potential (V). Equation 4 has been used for simulations of DBS [57, 81], modelling the brain as a heterogeneous medium with frequency-dependent electric conductivities. Electric conductivities for the different brain tissue types at some common DBS frequencies are summarized in Table 2. It is seen that cell-containing tissue types, i.e. grey and white matter, have low, frequency-dependent conductivities, while the conductivities of CSF and blood are higher and independent of the applied frequency.

Table 2. Electric conductivities of different brain tissue types at three common DBS frequencies [77].

Tissue type	**Electric conductivity (S/m)**		
	f = 60 Hz	**f = 130 Hz**	**f = 200 Hz**
Grey matter	0.081	0.092	0.094
White matter	0.055	0.059	0.060
Blood	0.70	0.70	0.70
CSF	2.0	2.0	2.0

3.3 Models and simulations

3.3.1 FEM models

In this thesis, commercial FEM software (Comsol Multiphysics 3.5, Comsol AB, Sweden) was used to simulate analyte diffusion and electric currents in the brain. For the diffusion simulations, Equation 2 was used as the governing equation, with D, λ and k as user-defined input parameters. Geometric microdialysis catheter models based on CMA65 (10 mm length, 0.4 mm diameter; for details see Section 3.1.2), surrounded by a brain tissue domain, were set up. Equation 4 was used as governing equation for the electric simulations, with σ as input parameter. DBS electrode models based on Medtronics 3389 (1.27 mm diameter; for details see Section 3.1.2) were created and positioned in the brain tissue domain. The boundary and initial conditions for the simulations are summarized in Figure 11.

For statistical evaluation of the TVI_{max} (Paper I), a FEM model was set up in an axi-symmetric co-ordinate system. The FEM model included a brain tissue domain modelled as a cylinder, with a height of 20 mm and radius of 10 mm. All tissue and analyte related properties were varied within physiologically relevant intervals, as described in Section 3.3.2. For simulation and visualization of the TVI_{max} and the DBS electric field in relation to patient anatomy (Paper I-III), patient-specific FEM models were set up in a three-dimensional Cartesian co-ordinate system. In each model, the geometry of the surrounding brain tissue was represented with a rectangle, 60x40x40 mm for Paper I and Paper II and 80x80x55 mm for Paper III. The dimensions of the brain tissue domains were set in order to include all basal ganglia structures of interest, i.e. the putamen, the GP, the internal capsule and the STN. The positioning of the electrode and catheter models and the assignment of input parameters to each FEM model was based on the intensity and property matrices described in Section 3.3.2.

3.3.2 Property matrices and model input parameters

MATLAB-based software developed by our group (ELMA1.0 [57, 82]) was used in order to set up image-based intensity and property matrices to be applied to the brain tissue domain for the FEM simulations. The software was used to relate the pre- and postoperative data sets to each other, segment and classify the patient images and assign physical properties such as electric conductivity and diffusivity to each voxel. Each type of intensity and property matrix

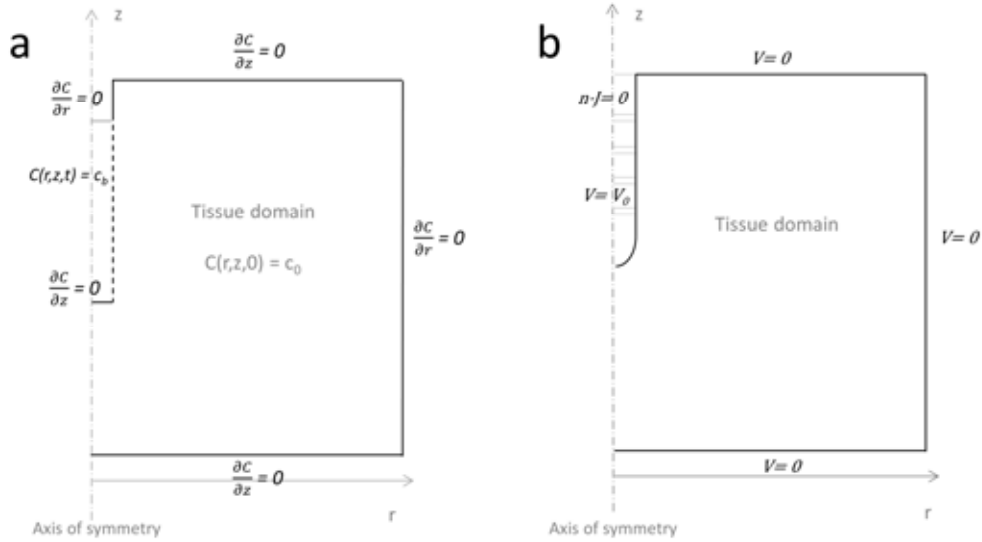

Figure 11. Initial and boundary conditions for the simulation of **a)** the TVImax and **b)** the DBS electric fields. Governing equations are denoted in bold, boundary conditions in italic and initial conditions in grey. In a), C is the analyte concentration (nmol/L), D is the diffusion coefficient (cm^2/s), λ is the tissue tortuosity, k is the clearance constant (s^{-1}) and c_b is the analyte concentration at the catheter boundary. In b), J is the current density (A m^{-2}), V is the electric potential (V), V_0 is the electric potential at the active electrode contact(s) and σ is the tissue conductivity (S m^{-1}).

is described below, together with the specific input parameters used for each FEM model. An overview of all intensity and property matrices is provided in Figure 12.

Intensity matrix for electrode and catheter positioning

For the patients in Paper I-II, the postoperative stereotactic CT images were used to create an intensity matrix for placement of the modeled electrodes and catheters at their true patient-specific positions. The positioning was made possible due to image artefacts originating from the DBS electrodes and the gold markers in the tips of the microdialysis catheters. Calculations were performed, based on the frame fiducial co-ordinates in the pre-and postoperative images, for transfer of the electrode and catheter positions to the MRI intensity matrix.

Intensity matrix for tissue visualization

For all patient-specific simulations (Paper I-III), the preoperative stereotactic MRI images were used to create patient-specific intensity matrices for visualization of patient anatomy in the FEM software. Each voxel was represented in the simulation software with an intensity value, interpolated from the original MRI image.

Diffusivity matrix

For the diffusion simulations, a matrix was set up to represent the effective diffusivity in each voxel of the brain tissue model. In Paper I and II, the target areas for the catheters were the putamen and the GPi, which were considered to consist of isotropic, grey matter. Therefore, the diffusion in each voxel was represented by a scalar value corresponding to the effective diffusion coefficient of the substance of interest, $D_e = D/\lambda^2$. For Paper III, the diffusion in each voxel was represented by a second-order tensor $\boldsymbol{D_e}$, derived from the DTI data. In both cases, the loss rate constant k for the brain tissue domain was defined in the simulation software.

For the axi-symmetric model in Paper I, which was used for evaluation of the TVI_{max}, the three input parameter values (D, λ, k) were varied within physiologically relevant intervals, and a new matrix was set up for each value combination. The value of D was varied in steps between $4 \cdot 10^{-6}$ – $1 \cdot 10^{-5}$ cm^2/s to represent all analytes of interest, the values of λ were considered normally distributed with a mean of 1.59 and a standard deviation of 0.096 [71] and the values of k were assumed to be evenly distributed on the interval 0.003 – 0.010 s^{-1} [75, 83, 84]. For the three-dimensional FEM models in Paper I and Paper II, D was set to $7.5 \cdot 10^{-6}$ cm^2/s, λ was set to 1.6 and k was set to 0.0065 s^{-1}, representing average values for the tissue and analytes of interest [71, 75, 83, 84]. For the DTI-based simulations in Paper III, the mean effective diffusivity of each dataset was set to $1.95 \cdot 10^{-6}$, $2.92 \cdot 10^{-6}$ and $3.51 \cdot 10^{-6}$ cm^2/s, respectively, to represent diffusion of substances with D = 5, 7.5 and $9 \cdot 10^{-6}$ cm^2/s in a tissue medium with λ = 1.6. The value of k was set to 0.0065 s^{-1}.

Electric conductivity matrix

For the electric field simulations (Paper II), intensity-based segmentation of the MRI images was used for identification of different tissue types, and each tissue type was assigned a frequency-dependent value of σ based on Audreccetti's online database [79]. Some voxels may contain more than one tissue type, resulting in partial volume effects. Therefore, a linear interpolation function was used to assign approximated conductivity values to such voxels. This process has been described in detail by Åström et al [57]. For all patients in Paper II, a DBS frequency of 130 Hz was used, corresponding to σ values of 0.09 S/m for grey matter, 0.06 S/m for white matter, 0.70 S/m for blood and 2.0 S/m for CSF [79].

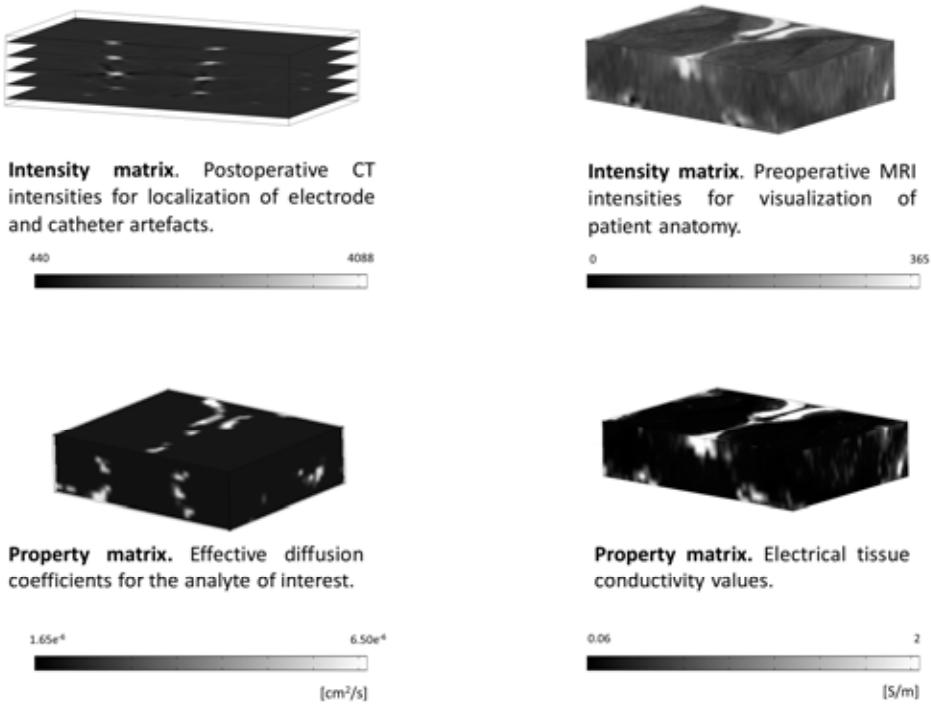

Figure 12. Overview of the intensity and property matrices used to represent the brain tissue domain for the FEM simulations.

3.3.3 Mesh and solver parameters

All meshes were automatically generated by the FEM software, with the highest mesh density around corners and edges close to the electrode and catheter models. To preserve the spatial resolution of the MRI and DTI data, the maximum element length was set to 1 mm in Paper I and II and to 1.5 mm in Paper III. The axi-symmetric FEM model (Paper I) was divided into about 3000 triangular mesh elements, while the three-dimensional models consisted of about 1,000,000 (Paper I-II) and 1,500,000 (Paper III) tetrahedral mesh elements, respectively. All models were solved using Comsol Multiphysics' iterative system solver *GMRES* with the preconditioner *Incomplete LU*.

3.4 Statistical methods

3.4.1 Factorial design

A factorial experiment explores how changing different independent variables, called factors, affects a defined response variable. Factorial designs can be used to study the effect of changing one parameter at a time, called main effects, as well as interactions between variables [85]. Factorial design was used in Paper I, to estimate the effect of three defined input parameters (D, λ and k) on the simulated analyte migration distance (r_{TVImax}). Since the experiment aimed to provide a rough overview of the impact of each input parameter, only the main effects were presented.

3.4.2 Regression analysis

In Paper I, regression analysis was carried out to model the simulated r_{TVImax} and its associated confidence interval as a function of D, with varying values of λ and k. Regression analysis is a method to study how one or more exposure variables x impact an outcome variable y. This is done by fitting a regression line to describe the association of points within a dataset, using least squares methods [86]. In the simplest form of regression analysis, called linear regression, the regression line is straight and is mathematically described as:

$$\hat{y} = \beta_0 + \sum_{k=1}^{n} \beta_k x_k \tag{5}$$

Here, $\hat{y}$ is the estimated response variable based on the exposure variable(s) x and the calculated regression coefficients β. Linear regression is based on the assumptions that the response variable $\hat{y}$ is normally distributed, and that the standard deviation is similar for all data points. If these assumptions are violated, mathematical operations such as logarithmic transformation are commonly applied to the dataset. Furthermore, if a straight regression line is considered insufficient to describe the points of the dataset, which can be tested by linear effect investigation, higher-order terms can be included in the model to improve the fit [86]. In Paper I, the following principal regression model was used:

$$\log\left(\hat{y}\right) = \beta_0 + \beta_1 x + \beta_2 x^2 \tag{6}$$

The goodness of fit of a regression model can be described by the coefficient of determination R^2, defined as:

$$R^2 = \frac{\sum_{k=1}^{n}(\hat{y}_i - \bar{y})^2}{\sum_{k=1}^{n}(\hat{y}_i - \bar{y})^2 + \sum_{k=1}^{n}(y_i - \bar{y})^2} \quad (7)$$

Here, y_i are the observed values, $\bar{y}$ is the mean value of the dataset and $\hat{y}_i$ are the values predicted by the model. The value of R^2 ranges between 0 and 1 and is related to the proportion of variation that can be explained by the regression model. $R^2 = 0$ means that the variability of y cannot be explained at all by the model, while $R^2 = 1$ means that the model completely explains y [86].

3.4.3 Descriptive statistics

Descriptive statistics are used to quantitatively describe the main features of a collection of data, such as the average value of a dataset and the spread of the data around the average value [86]. It is particularly useful for providing summaries about a sample and the observations which have been made, without generalizing the conclusions to a whole population. Therefore, descriptive statistics were considered suitable for evaluation and presentation of the simulation data in Paper III, since data for only one human subject was used in the study.

4 Studies and results

4.1 Definition of the TVI_{max} (Paper I)

The primary aim of Paper I was to define and simulate the TVI_{max}, interpreted as a qualitative estimation of the maximum tissue volume from which biochemical data is obtained during brain microdialysis. When defining the TVI_{max}, the underlying assumption was that the maximum sampling distance for an analyte is equal to its maximum migration distance, given the same tissue and substance related parameters and a defined time interval. Under this assumption, the TVI_{max} was simulated using reverse microdialysis, i.e. release of the analyte from the catheter into the tissue. An axi-symmetric FEM model, as described in Section 3.3.1, was set up in order to simulate the defined TVI_{max}. The outer boundaries of the tissue domain were modelled as insulated, and the analyte release into the brain was included as a boundary condition at the catheter surface, as illustrated in Figure 11. The TVI_{max} was simulated using Equation 2, together with the assumptions stated in Paper I. The outer boundary was defined with a concentration isolevel at $C = 0.01c_b$, where c_b is the analyte concentration at the catheter boundary. The simulated TVI_{max} is illustrated in Figure 13.

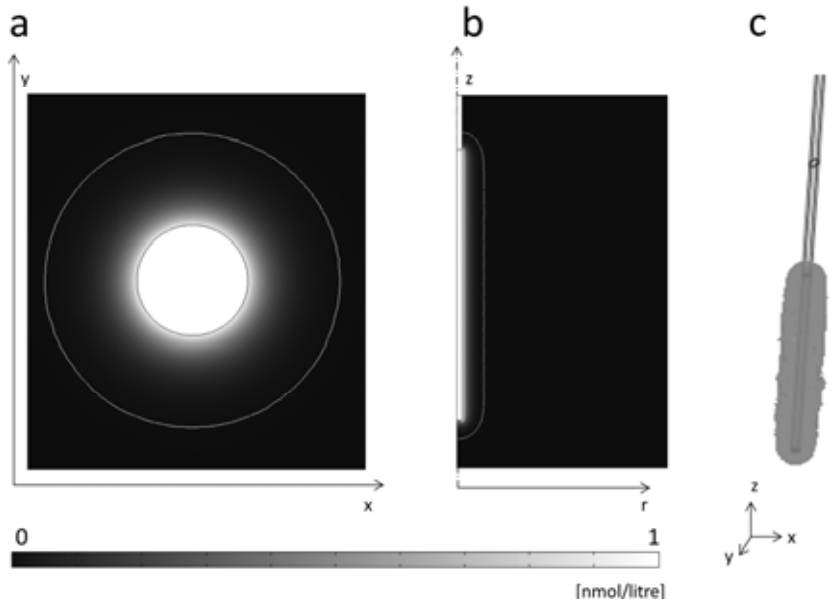

Figure 13. Different views of the simulated TVI_{max}, with the outer boundary seen as a bright line in figure **a)** - **b)**. **a)** Axial view **b)** Axi-symmetric view **c)** Three-dimensional view.

4.2 Evaluation of the TVI_{max} (Paper I and III)

For model evaluation, the cross-sectional radius of the TVI_{max} (the r_{TVImax}), corresponding to the maximum analyte migration distance from the catheter, was used as the main response variable. The simulated r_{TVImax} was evaluated by changing three model input parameters: the tortuosity λ, the analyte diffusision coefficient D and the loss rate constant k.

In Paper I, all input parameters for the simulation were modelled as scalar quantities, and two statistical evaluations were performed using relevant literature values (Section 3.3.2) as basis. First, a factorial design was used to evaluate the impact of each input parameter on the r_{TVImax}, concluding that the r_{TVImax} increases with an increasing value of D while decreasing for increased values of λ and k. Regression analysis was then used, to model the r_{TVImax} as a function of D with randomly varying values of λ and k. It was concluded that for a D value of $7.5 \cdot 10^{-6}$ cm^2/s, representing the neuroactive substances of interest, the r_{TVImax} was 0.85 mm with a 95% confidence interval ranging over about 0.5 mm. The large confidence interval originated from the range of relevant literature values found for λ and k.

In Paper III, the analyte diffusivity was represented by a tensor, $\boldsymbol{D_e}$, corresponding to the effective diffusivity of an analyte in an anisotropic tissue medium. Human DTI data was used to extract second-order tensors representing the diffusion of water of brain tissue. In this way, the effect of local brain anisotropy and heterogeneity on the TVI_{max} could be explored for different basal ganglia nuclei. Simulations based on DTI data affected the cross-sectional radius of the TVI_{max} by up to 0.5 mm (n = 98444), with the largest variations seen for the subthalamic area and the internal capsule which are crossed by white matter tracts. It was also seen that the mean value of the r_{TVImax} was about 5% smaller for the DTI-based models compared to the corresponding isotropic references.

4.3 Ex vivo evaluation (Paper I)

A microdialysis experiment was performed on brain tissue from calf obtained from the local slaughterhouse (use approved by the Swedish Board of Agriculture, D.O. 38-172/09) in order to estimate diffusion in the deep brain structures and compare it to the simulation results. A microdialysis catheter (10 mm length, 0.4 mm diameter; for details see Section 3.1.2) was introduced into the brain tissue, and perfused with crystal violet solution ($D = 4.2 \cdot 10^{-6}$ cm^2/s) for one hour. The tissue was cut in 1 mm thick slices perpendicular to the catheter membrane,

and the cross-sectional radius of the coloured surface corresponding to the migration of crystal violet was compared to the simulated r_{TVImax}. A cross-sectional radius of 0.64 ± 0.08 mm was seen for the crystal violet diffusion, which was in good agreement with the regression model prediction for a substance with a similar value of *D* (Figure 14).

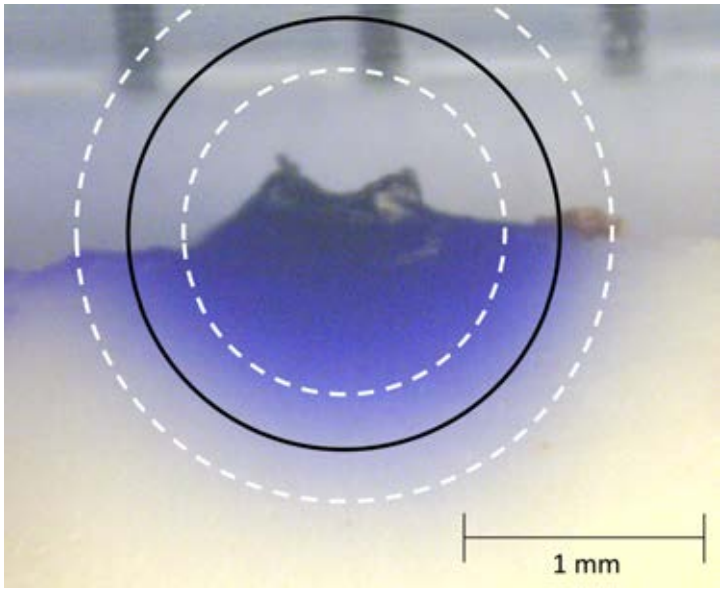

Figure 14. Coloured surface resulting from the ex vivo microdialysis experiment. The cross-section of the TVI_{max}, as calculated by regression analysis, is included as a black line, with the associated 95% confidence interval traced in white.

4.4 Patient-specific simulations and visualizations (Paper I and II)

In Paper I, the TVI_{max} was simulated in relation to patient anatomy for four patients with PD, all undergoing microdialysis in parallel to DBS. The patient data and clinical procedure are described in Section 3.1, while the simulation procedure and the model input parameters are described in Section 3.3.1 and 3.3.2. Axial MRI slices were used together with the outlines of the modelled TVI_{max} of each catheter and extracted brain atlas contours, in order to provide a spatial overview of the TVI_{max} in relation to anatomical structures (Figure 15). Using the catheter positions and the simulated TVI_{max} as basis, the microdialysis data could be related to one main nucleus for each catheter. For two out of four patients, it could be confirmed that the biochemical data was obtained from the targets aimed at, namely the right putamen and the

left and right GPi. For the third patient, one catheter was placed between the GPi and the GPe rather than within the GPi. For the fourth patient, two out of three catheters were placed outside of the intended targets; the right GPe was sampled rather than the right GPi and the left SN was sampled rather than the left GPi.

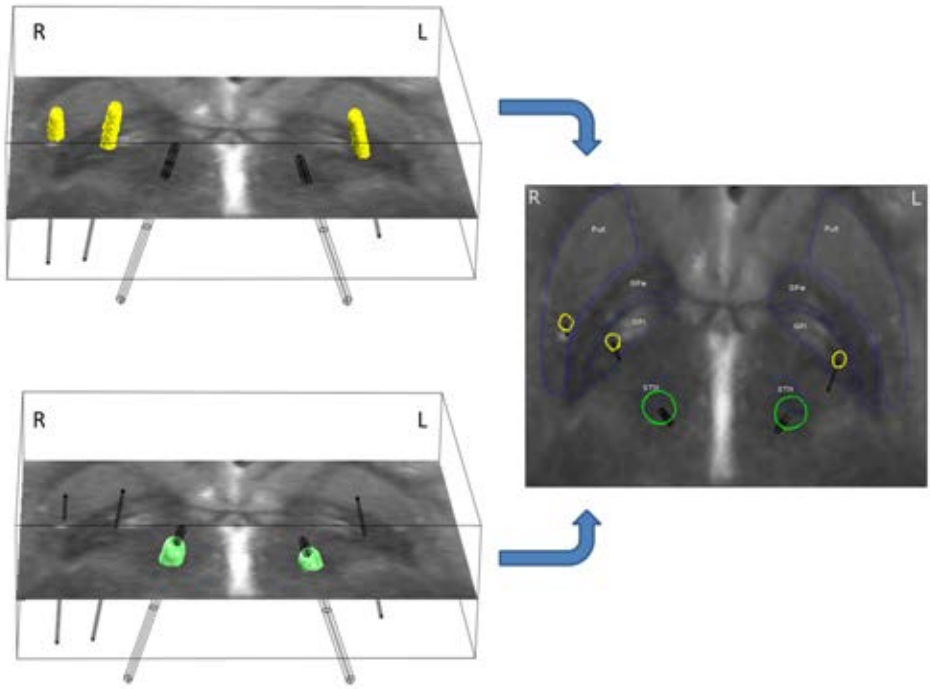

Figure 15. Simulation and visualization of the TVI_{max} (upper left) and the DBS electric fields (lower left) in relation to patient anatomy. The right image shows an axial MRI slice with outlines of the simulated TVI_{max} and electric fields, together with superimposed brain atlas structures [8, 87].

In Paper II, the patient-specific models from Paper I were combined with simulations of the electric field surrounding the DBS electrodes. Tissue-specific electric conductivities, as described in Section 3.3.2, were introduced together with geometric models of the DBS electrodes. The electric potential delivered from each DBS electrode was included as a boundary condition, as shown in Figure 11, with magnitude and active contacts set according to the clinically used parameters (Table I in Paper II). The electric field around each DBS electrode was simulated and visualized, together with the TVI_{max} and the MRI images for each patient. An isolevel at 0.2 V/mm was used for electric field visualization [57, 59]. The

dorsomedial STN turned out to be the main stimulation target for three of the patients, while the stimulation was focused around the SN for the fourth patient.

4.5 Relation to clinical data (Paper I)

In Paper I, the obtained microdialysis data for dopamine ($D = 7.5 \cdot 10^{-6}$ cm^2/s) for one of the patients was included, and related to the patient-specific simulation. The simulation showed that the TVI_{max} for each catheter was restricted to one main anatomical target area, in this case confirming that the intended nuclei had been sampled. Following DBS, an increased concentration of dopamine was observed for the catheter placed in the putamen, but not for the two catheters placed in the GPi. This result indicated that there are differences in the biochemical signaling between the sampled targets, thereby highlighting the need to define the catheter position and the associated TVI_{max}.

5 Discussion and conclusions

The overall aim of this thesis was to use FEM simulations, together with physiologically relevant parameter values, in order to estimate and visualize the tissue volume of influence during microdialysis of the basal ganglia. Such simulations were combined with patient-specific image data, in order to predict the anatomical structures which are being sampled during a microdialysis experiment. Furthermore, it was demonstrated how analyte diffusion simulations and electric field simulations can be combined when using microdialysis in parallel to DBS. In this way, the biochemical data can be related to their anatomic origin as well as to the electric stimulation, thereby potentially improving the understanding of the biochemical signalling pathways in relation to DBS treatment.

5.1 Definition of the TVI_{max}

The TVI_{max} is used to provide a qualitative approximation of the maximum tissue volume that can be sampled during a brain microdialysis experiment. This is done by simulating the analyte migration in all directions from the microdialysis catheter, using D, λ and k as input parameters. The underlying assumption for the simulation of reverse microdialysis is that the analyte is continuously released into and removed from the tissue, which is true for the neuroactive substances involved in the signaling pathways of the basal ganglia [1, 4]. The input parameters used in this thesis are similar to those proposed by Bungay et al [88] in order to define the spatial penetration depth of microdialysis. As concluded in Paper I, the mean r_{TVImax} for a substance with $D = 7.5 \cdot 10^{-6}$ cm^2/s, representing the neurotransmitters of interest, shows good agreement with the penetration depth predicted by Bungay et al [88] when a similar concentration isolevel is used.

It should be clearly pointed out that the TVI_{max} only provides a qualitative estimation of the maximum sampling volume for a microdialysis catheter. A quantitative estimation would require detailed knowledge about the interaction between the analyte and the surrounding brain tissue in a particular tissue volume, and obtaining such data on a patient-specific basis is not possible. Also, the influence of catheter-related parameters such as membrane properties and flow rate [89] are not taken into account in the current models. Such parameters may affect the shape and the size of the TVI_{max}, and should be considered if a more careful

evaluation of the interaction between the catheter and the surrounding tissue during brain microdialysis is made. Developing a more detailed model which takes further technical aspects into account is a possible subject for future studies.

For the statistical evaluations of the TVI_{max} (Paper I and Paper III), its cross-sectional radius has been considered more relevant as a response variable than the actual volume. This is because the r_{TVImax} corresponds directly to the maximum analyte migration distance, allowing interpretation of the analyte diffusion in relation to the geometrical dimensions of surrounding anatomical structures. The r_{TVImax} is also closely related to the microdialysis penetration depth, which has been evaluated in previous studies [88-90]. In future studies, the extension of the TVI_{max} along the catheter membrane should be more carefully considered – when sampling small targets such as the STN with a maximum width of about 10 mm [91], the catheter length may exceed the depth of the nuclei of interest. In such cases, the anatomical structures superior and inferior to the STN, such as the SN and the thalamus, may influence the biochemical data.

5.2 Model input parameters

The values of the microdialysis model input parameters are based on previous studies and reviews [71, 75, 84, 92], and are intended to reflect physiologically relevant intervals. The parameter intervals used for evaluation of the TVI_{max} are intentionally large, in order to account for all variations that may occur due to differences between different brain regions and brain-analyte interactions. Based on literature values and regression analysis (Paper I), the r_{TVImax} for a neurotransmitter can be simulated with a certainty of ± 0.25 mm, although possibly overestimated in some basal ganglia regions because of the uncertainty and potential underestimation of k. When simulating the maximum volume of influence, an overestimation is clearly preferred over an underestimation, and the TVI_{max} is generally small enough to limit the data from each catheter to one anatomical structure (Paper I, Paper III). The potential overestimation of the TVI_{max} provides a disadvantage in some cases, such as for Patient 2 in Paper I; a more detailed estimation of the input parameters would here be required in order to limit the TVI_{max} to one target or estimate the influence from each target. The analyte diffusion may also be influenced by parameters not included in the model; bulk flow has been proposed to influence the diffusion in the perivascular spaces and fiber tracts of the brain, for example, although its existence and magnitude are subject to debate [74].

The use of DTI data to model and simulate anisotropic and heterogeneous diffusion in brain tissue (Paper III) has only been used in a few previous studies [47, 48]. Future experimental studies are suitable in order to further validate the findings presented here. The hypothesis that DTI data accurately reflects the diffusion properties of brain tissue is supported by multiple studies, [44, 46, 93, 94], and using DTI for patient-specific diffusion simulations provides an advantage over an isotropic assumption. Furthermore, the results from Paper III are reasonable in relation to the expected variation of the analyte diffusivity [71], and the current knowledge of the basal ganglia. DTI images are not routinely obtained for patients undergoing DBS, and the results obtained in Paper III should be seen as guidelines for the variation of the TVI_{max} that may be caused by brain tissue anisotropy and heterogeneity in different basal ganglia structures. Such guidelines should be used in future microdialysis simulation studies if isotropic assumptions are made.

5.3 Ex vivo evaluation

In order to relate the simulation results to experimental data, an ex vivo brain microdialysis experiment was considered appropriate (Paper I). Agreement was seen between the simulation data and the experimental values, indicating that the prediction of the TVI_{max} is reasonable. Only one substance was used for the experimental study; to increase the validity of the experiment, a future study involving multiple substances would be suitable. There is one significant difference between in vivo and ex vivo brain studies; part of the analyte clearance from the extracellular space is due to removal through capillary blood flow [71], and the absence of blood flow in ex vivo samples will likely decreases the value of k. The value of λ, on the other hand, may increase in ex vivo tissue samples as a consequence of tissue ischemia and cell swelling [95]. The fact that the experimental values are in agreement with the simulation data does not guarantee that each parameter value agrees with that theoretically predicted.

5.4 Patient-specific simulations

Basal ganglia structures are in the millimetre range connected by multiple neural pathways [96], and the clinical data provided in Paper I indicate that there are differences in the biochemical response to DBS among the target areas. Confirmation of the microdialysis target area is therefore crucial when interpreting the obtained data and comparing them between

patients. Patient-specific simulations and visualizations of the TVI_{max} provide information about the tissue volume that is being sampled during a microdialysis experiment, allowing interpretation of the data in relation to anatomical targets. By combining the diffusion simulations with patient-specific DBS simulations, the biochemical data can also be related to the DBS target area.

In Paper II, the simulations of the TVI_{max} were combined with a method for DBS electric field simulations based on a method previously developed in our group. This method has been described and evaluated in a number of previous studies [50, 57, 82, 97], and the electric field simulation part has therefore been kept short in order to keep the main focus on the microdialysis simulations. An isolevel at 0.2 V/mm was used for visualization of the electric fields generated by DBS; this isolevel is thought to lie within the volume of neural activation for standard DBS parameters [98]. The isolevel was initially proposed by Hemm et al. [59], and was later found suitable by Åström et al. [97] to investigate speech-related side effects during DBS of the STN. The simulations of the DBS electric fields in this study should be seen as rough overviews, allowing comparisons between the patients without drawing extensive conclusions about the surrounding neuronal environment. This is in contrast to the work of Butson et al. [52, 58] where DBS electric field simulations were combined with models of the surrounding neurons in order to predict the volume of tissue activated during DBS.

The simulations presented in this thesis provide estimations of the field quantities of interest, and these estimations are affected by several assumptions and limitations. Possible sources of error include the isotropic tissue assumption made in Paper I and II, the limited image resolution for the MRI and DTI images, MRI and CT image artefacts, the manual MRI-based segmentation of different tissue types, the choice of model input parameter values and round-off errors originating from the simulation software. Because of the potential influence of such errors, the simulation results have been described on an overview level to allow comparisons between the different brain targets and patients.

5.5 Clinical data

How DBS exerts its therapeutic effects is still debated and different mechanisms of action have been proposed. It has been shown that DBS of the STN often reduces the need for oral

levodopa and may induce dyskinesias [99, 100], and the mechanisms behind these clinical observations may be related to alterations in the levels of neurotransmittors in the basal ganglia. Studying the relationship between the TVI_{max} for each microdialysis catheter, the electric field generated by the DBS electrodes, and the variations in the neurotransmitter concentrations may improve the individualized and patient-specific DBS treatment. The dopamine plot shown in Paper I is part of a current study [101], where biochemical data for multiple neuroactive substances is analyzed in relation to DBS. Altogether, four patients have been included in the study and several neurotransmitters and related substances are to be analyzed. The developed FEM models will be used for patient-specific predictions of the TVI_{max} and the DBS electric fields, facilitating interpretation of the results.

5.6 Conclusions and future directions

In the current thesis, it has been shown how diffusion FEM simulations can be combined with patient-specific images and clinical data, in order to improve the interpretation of brain microdialysis data in relation to DBS. Although the accuracy of the diffusion simulations may be limited by both known and unknown sources, the TVI_{max} showed to be suitable for relating the data of a microdialysis catheter to one main target area. Furthermore, it was demonstrated how such diffusion simulations can be combined with patient-specific simulations of the electric fields generated by DBS electrodes. By providing an overview of the anatomical structures possibly influencing the microdialysis measurements, as well as those affected by the electric stimulation, such simulations may constitute an important step in the process of mapping and clarifying the mechanisms behind DBS.

The simulation of the TVI_{max} depends on parameters associated with the analyte and tissue of interest, and the parameter values used in this thesis were based on relevant literature-based intervals. FEM is a flexible method allowing model refinement as well as introduction of additional input parameters, so all parameter values and assumptions used in this thesis can be changed and refined if needed for future studies. This allows further development of the current application, as well as adaptation of the microdialysis FEM model to other applications, analytes and tissues. Prediction of tissue properties during immunological skin microdialysis studies and estimation of the TVI_{max} for trauma patients during neuro-intensive care are two examples of clinical applications where the developed model can be used.

The works included in this thesis have been performed in an interdisciplinary manner, involving engineers, neurosurgeons, neurologists and biochemists. The combination of technical and clinical knowledge and experience facilitates the development of suitable patient-specific computer models which are useful for evaluation of clinical data. Future interdisciplinary work should focus on the relation between the clinical data and the simulation results, as well as further studies involving larger patient groups, in order to contribute to the mapping of the mechanisms underlying DBS. Further knowledge about the effects of DBS in relation to basal ganglia connections may aid the clinicians in the preoperative planning as well as the postoperative follow-up control, thereby contributing to improving the quality of life for patients with movement disorders.

Acknowledgments

There are many people who have contributed to this thesis, by providing knowledge and experience as well as inspiration and encouragement. First of all, I would like to thank my supervisor, Karin Wårdell, for her positive attitude, support and encouragement, and my co-supervisor, Mats Andersson, for his scientific contributions and support. Thanks also to my research group, the MINT group, with a special thanks to Mattias Åström and Johannes Johansson who have taught me a lot about the specific research topics of this thesis. Furthermore, I would like to thank Nil Dizdar, Anita Kullman and Peter Zsigmond, co-authors of Paper I and II, for providing clinical knowledge and experience. It has been fun and interesting to work together, and I have learned a lot from you. I also owe a special thanks to Dan Loyd, who has contributed with valuable technical knowledge as well as inspiration and encouragement.

I would also like to thank my colleagues at the Department of Biomedical Engineering, for providing a nice and inspiring work environment. A special thanks to my "fika-buddies" (Joakim, Linda, Peter, Hanna, Martin, Micke and many others) for making the 10 o'clock coffee break one of the highlights of the day.

Most importantly, I would like to thank my parents, my brother and my boyfriend Magnus, for your love and support and for always believing in me. Thanks also to my beloved friends outside of work, in particular to my current Linköping friends (Sarah, Frida, Karin, Christian, Herman, Eric, Stefan and others) – life in Linköping would really not be that great if you were not part of it.

I would also like to acknowledge the financial support that made this thesis possible, provided by the Swedish Governmental Agency for Innovation Systems (Vinnova), Swedish Foundation for Strategic Research (SSF), Swedish Research Council (VR) (Group grant no. 311-2006-7661), Research Foundation of the County Council of Östergötland, Medical Research Council of Southeast Sweden and Linköping University´s Foundation for Parkinson's Research.

References

1. Tortora, G.J. and B. Derrickson, *Principles of anatomy and physiology*. 12th ed2010, Hoboken, NJ: John Wiley & Sons.
2. Connors, B.W., *Physiology of Neurons*, in *Medical physiology : a cellular and molecular approach*, W.F. Boron and E.L. Boulpaep, Editors. 2009, Saunders/Elsevier: Philadelphia, PA.
3. Connors, B., *Synaptic Transmission in the Nervous System*, in *Medical Physiology*, W.F. Boron and E.L. Boulpaep, Editors. 2003, Elsevier Science: Philadelphia.
4. Ransom, B.R., *The Neuronal Microenvironment*, in *Medical physiology : a cellular and molecular approach*, W.F. Boron and E.L. Boulpaep, Editors. 2009, Saunders/Elsevier: Philadelphia, PA.
5. Mellander, S., *Perifer cirkulation. Blodkärlens fysiologi*1976: Sandoz AB.
6. Charara, A., Sidibe, M., Smith, Y., *Basal Ganglia Circuitry and Synaptic Connectivity*, in *Clinical Neurology: Surgical Treatment of Parkinson´s Disease and Other Movement Disorders*, D. Tarsy, Vitek, J.L., Lozano, A.M., Editor 2003, Humana Press Inc: Totowa, NJ.
7. Ma, T.P., *The Basal Nuclei*, in *Fundamental Neuroscience*, D.E. Haines, Editor 2002, Churchill Livingstone: New York.
8. Nolte, J., *The human brain : an introduction to its functional anatomy*. 6th ed2009, Philadelphia, PA: Mosby/Elsevier. xii, 720 p.
9. Barone, P., *Neurotransmission in Parkinson's disease: beyond dopamine.* European Journal of Neurology, 2010. **17**(3): p. 364-376.
10. Benabid, A.L., *Deep brain stimulation for Parkinson's disease.* Curr Opin Neurobiol, 2003. **13**(6): p. 696-706.
11. Montgomery, E.B., Jr. and J.T. Gale, *Mechanisms of action of deep brain stimulation(DBS).* Neurosci Biobehav Rev, 2008. **32**(3): p. 388-407.
12. McIntyre, C.C. and P.J. Hahn, *Network perspectives on the mechanisms of deep brain stimulation.* Neurobiol Dis, 2009.
13. Dorsey, E.R., R. Constantinescu, J.P. Thompson, K.M. Biglan, R.G. Holloway, K. Kieburtz, F.J. Marshall, B.M. Ravina, G. Schifitto, A. Siderowf, et al., *Projected number of people with Parkinson disease in the most populous nations, 2005 through 2030.* Neurology, 2007. **68**(5): p. 384-6.
14. Jankovic, J., *Parkinson's disease: clinical features and diagnosis.* Journal of Neurology Neurosurgery and Psychiatry, 2008. **79**(4): p. 368-376.
15. Wirdefeldt, K., H.O. Adami, P. Cole, D. Trichopoulos, and J. Mandel, *Epidemiology and etiology of Parkinson's disease: a review of the evidence.* European Journal of Epidemiology, 2011. **26**: p. S1-S58.
16. Modolo, J. and A. Beuter, *Linking brain dynamics, neural mechanisms, and deep brain stimulation in Parkinson's disease: An integrated perspective.* Medical Engineering & Physics, 2009. **31**(6): p. 615-623.
17. Grosset, D.G., K.A. Grosset, M.S. Okun, and H.H. Fernandez, *Parkinson´s Disease*2009, London: Manson Publishing Ltd.
18. Benabid, A.L., S. Chabardes, J. Mitrofanis, and P. Pollak, *Deep brain stimulation of the subthalamic nucleus for the treatment of Parkinson's disease.* Lancet Neurol, 2009. **8**(1): p. 67-81.
19. Johnson, M.D., S. Miocinovic, C.C. McIntyre, and J.L. Vitek, *Mechanisms and targets of deep brain stimulation in movement disorders.* Neurotherapeutics, 2008. **5**(2): p. 294-308.
20. Hemm, S. and K. Wårdell, *Stereotactic implantation of deep brain stimulation electrodes: a review of technical systems, methods and emerging tools.* Med Biol Eng Comput, 2010. **48**(7): p. 611-24.

21. Albert, G.C., C.M. Cook, F.S. Prato, and A.W. Thomas, *Deep brain stimulation, vagal nerve stimulation and transcranial stimulation: An overview of stimulation parameters and neurotransmitter release.* Neurosci Biobehav Rev, 2009. **33**(7): p. 1042-60.
22. Machado, A., A.R. Rezai, B.H. Kopell, R.E. Gross, A.D. Sharan, and A.L. Benabid, *Deep brain stimulation for Parkinson's disease: surgical technique and perioperative management.* Mov Disord, 2006. **21 Suppl 14**: p. S247-58.
23. Kuncel, A.M. and W.M. Grill, *Selection of stimulus parameters for deep brain stimulation.* Clin Neurophysiol, 2004. **115**(11): p. 2431-41.
24. Gross, R.E., P. Krack, M.C. Rodriguez-Oroz, A.R. Rezai, and A.L. Benabid, *Electrophysiological mapping for the implantation of deep brain stimulators for Parkinson's disease and tremor.* Movement disorders : official journal of the Movement Disorder Society, 2006. **21 Suppl 14**: p. S259-83.
25. Zrinzo, L.U. and M.I. Hariz, *Impedance recording in functional neurosurgery*, in *Textbook of stereotactic and functional neurosurgery*, A.M. Lozano, P.L. Gildenberg, and R.R. Tasker, Editors. 2008, Springer: Berlin.
26. Johansson, J.D., P. Blomstedt, N. Haj-Hosseini, A.T. Bergenheim, O. Eriksson, and K. Wårdell, *Combined diffuse light reflectance and electrical impedance measurements as a navigation aid in deep brain surgery.* Stereotactic and functional neurosurgery, 2009. **87**(2): p. 105-13.
27. Blomstedt, P. and M.I. Hariz, *Hardware-related complications of deep brain stimulation: a ten year experience.* Acta neurochirurgica, 2005. **147**(10): p. 1061-4; discussion 1064.
28. Smith, M.J. and M.G. Kaplitt, *Microdialysis*, in *Textbook of Stereotactic and Functional Neurosurgery*, A.M. Lozano, P.L. Gildenberg, and R.R. Tasker, Editors. 2009, Springer: Berlin.
29. Tisdall, M.M. and M. Smith, *Cerebral microdialysis: research technique or clinical tool.* British journal of anaesthesia, 2006. **97**(1): p. 18-25.
30. Hillman, J., O. Aneman, C. Anderson, F. Sjögren, C. Saberg, and P. Mellergård, *A microdialysis technique for routine measurement of macromolecules in the injured human brain.* Neurosurgery, 2005. **56**(6): p. 1264-8; discussion 1268-70.
31. Galati, S., P. Mazzone, E. Fedele, A. Pisani, A. Peppe, M. Pierantozzi, L. Brusa, D. Tropepi, V. Moschella, M. Raiteri, et al., *Biochemical and electrophysiological changes of substantia nigra pars reticulata driven by subthalamic stimulation in patients with Parkinson's disease.* Eur J Neurosci, 2006. **23**(11): p. 2923-8.
32. Stefani, A., E. Fedele, S. Galati, M. Raiteri, O. Pepicelli, L. Brusa, M. Pierantozzi, A. Peppe, A. Pisani, G. Gattoni, et al., *Deep brain stimulation in Parkinson's disease patients: biochemical evidence.* J Neural Transm Suppl, 2006(70): p. 401-8.
33. Kilpatrick, M., E. Church, S. Danish, M. Stiefel, J. Jaggi, C. Halpern, M. Kerr, E. Maloney, M. Robinson, I. Lucki, et al., *Intracerebral microdialysis during deep brain stimulation surgery.* Journal of neuroscience methods, 2010. **190**(1): p. 106-11.
34. Zsigmond, P., N. Dernroth, A. Kullman, L.E. Augustinsson, and N. Dizdar, *Stereotactic microdialysis of the basal ganglia in Parkinson's disease.* Journal of neuroscience methods, 2012. **207**(1): p. 17-22.
35. Plock, N. and C. Kloft, *Microdialysis - theoretical background and recent implementation in applied life-sciences.* European Journal of Pharmaceutical Sciences, 2005. **25**(1): p. 1-24.
36. Farnebo, S., *On microvascular blood flow assessment with the new microdialysis urea clearance technique*, in *Department of Clinical and Experimental Medicine*2010, Linköping University: Linköping.
37. Ungerstedt, U., *Microdialysis--principles and applications for studies in animals and man.* J Intern Med, 1991. **230**(4): p. 365-73.
38. Hillman, J., P. Milos, Z.Q. Yu, F. Sjögren, C. Anderson, and P. Mellergård, *Intracerebral microdialysis in neurosurgical intensive care patients utilising catheters with different molecular cut-off (20 and 100 kD).* Acta neurochirurgica, 2006. **148**(3): p. 319-24; discussion 324.

39. Chefer, V.I., A.C. Thompson, A. Zapata, and T.S. Shippenberg, *Overview of brain microdialysis.* Current protocols in neuroscience / editorial board, Jacqueline N. Crawley ... [et al.], 2009. **Chapter 7**: p. Unit7 1.
40. Westerink, B.H.C. and W. Timmerman, *Do neurotransmitters sampled by brain microdialysis reflect functional release?* Analytica Chimica Acta, 1999. **379**(3): p. 263.
41. Elmaoglu, M., *MRI Handbook: MR Physics, Patient Positioning, and Protocols*. Vol. 1. 2011, New York: Springer-Verlag.
42. Edelman, R.R. and S. Warach, *Medical Progress .1. Magnetic-Resonance-Imaging.* New England Journal of Medicine, 1993. **328**(10): p. 708-716.
43. Le Bihan, D., *Looking into the functional architecture of the brain with diffusion MRI.* Nature Reviews Neuroscience, 2003. **4**(6): p. 469-480.
44. Le Bihan, D., J.F. Mangin, C. Poupon, C.A. Clark, S. Pappata, N. Molko, and H. Chabriat, *Diffusion tensor imaging: Concepts and applications.* Journal of Magnetic Resonance Imaging, 2001. **13**(4): p. 534-546.
45. Jellison, B.J., A.S. Field, J. Medow, M. Lazar, M.S. Salamat, and A.L. Alexander, *Diffusion tensor imaging of cerebral white matter: a pictorial review of physics, fiber tract anatomy, and tumor imaging patterns.* AJNR. American journal of neuroradiology, 2004. **25**(3): p. 356-69.
46. Basser, P.J. and C. Pierpaoli, *Microstructural and physiological features of tissues elucidated by quantitative-diffusion-tensor MRI.* Journal of magnetic resonance. Series B, 1996. **111**(3): p. 209-19.
47. Linninger, A.A., M.R. Somayaji, M. Mekarski, and L. Zhang, *Prediction of convection-enhanced drug delivery to the human brain.* Journal of theoretical biology, 2008. **250**(1): p. 125-38.
48. Linninger, A.A., M.R. Somayaji, T. Erickson, X. Guo, and R.D. Penn, *Computational methods for predicting drug transport in anisotropic and heterogeneous brain tissue.* Journal of biomechanics, 2008. **41**(10): p. 2176-87.
49. Tuch, D.S., V.J. Wedeen, A.M. Dale, J.S. George, and J.W. Belliveau, *Conductivity tensor mapping of the human brain using diffusion tensor MRI.* Proceedings of the National Academy of Sciences of the United States of America, 2001. **98**(20): p. 11697-701.
50. Åström, M., J.-J. Lemaire, and K. Wårdell, *Computational analysis of the influence of heterogeneous and anisotropic tissue on deep brain stimulation.* Submitted, 2010.
51. McIntyre, C.C., S. Mori, D.L. Sherman, N.V. Thakor, and J.L. Vitek, *Electric field and stimulating influence generated by deep brain stimulation of the subthalamic nucleus.* Clinical neurophysiology : official journal of the International Federation of Clinical Neurophysiology, 2004. **115**(3): p. 589-95.
52. Butson, C.R., S.E. Cooper, J.M. Henderson, and C.C. McIntyre, *Predicting the effects of deep brain stimulation with diffusion tensor based electric field models.* Med Image Comput Comput Assist Interv, 2006. **9**(Pt 2): p. 429-37.
53. Kalender, W.A., *Computed Tomography*, ed. D. Gunia. Vol. 3. 2011, Erlangen: Publicis Publishing.
54. Brenner, D.J. and E.J. Hall, *Current concepts - Computed tomography - An increasing source of radiation exposure.* New England Journal of Medicine, 2007. **357**(22): p. 2277-2284.
55. Liu, G.R. and S.S. Quek, *The finite element method : a practical course*2003, Oxford ; Boston: Butterworth-Heinemann. xv, 348 p.
56. Kaazempur-Mofrad, M.R., M. Bathe, H. Karcher, H.F. Younis, H.C. Seong, E.B. Shim, R.C. Chan, D.P. Hinton, A.G. Isasi, A. Upadhyaya, et al., *Role of simulation in understanding biological systems.* Computers & Structures, 2003. **81**(8-11): p. 715-726.
57. Åström, M., L.U. Zrinzo, S. Tisch, E. Tripoliti, M.I. Hariz, and K. Wårdell, *Method for patient-specific finite element modeling and simulation of deep brain stimulation.* Med Biol Eng Comput, 2009. **47**(1): p. 21-8.

58. Butson, C.R., S.E. Cooper, J.M. Henderson, and C.C. McIntyre, *Patient-specific analysis of the volume of tissue activated during deep brain stimulation.* Neuroimage, 2007. **34**(2): p. 661-70.
59. Hemm, S., G. Mennessier, N. Vayssiere, L. Cif, H. El Fertit, and P. Coubes, *Deep brain stimulation in movement disorders: stereotactic coregistration of two-dimensional electrical field modeling and magnetic resonance imaging.* J Neurosurg, 2005. **103**(6): p. 949-55.
60. Oshima, M., R. Torii, T. Kobayashi, N. Taniguchi, and K. Takagi, *Finite element simulation of blood flow in the cerebral artery.* Computer Methods in Applied Mechanics and Engineering, 2001. **191**(6-7): p. 661-671.
61. Taylor, C.A., T.J.R. Hughes, and C.K. Zarins, *Finite element modeling of blood flow in arteries.* Computer Methods in Applied Mechanics and Engineering, 1998. **158**(1-2): p. 155-196.
62. Kalyanasundaram, S., V.D. Calhoun, and K.W. Leong, *A finite element model for predicting the distribution of drugs delivered intracranially to the brain.* American Journal of Physiology-Regulatory Integrative and Comparative Physiology, 1997. **273**(5): p. R1810-R1821.
63. Johansson, J.D., O. Eriksson, J. Wren, D. Loyd, and K. Wårdell, *Radio-frequency lesioning in brain tissue with coagulation-dependent thermal conductivity: modelling, simulation and analysis of parameter influence and interaction.* Medical & Biological Engineering & Computing, 2006. **44**(9): p. 757-766.
64. Wren, J., O. Eriksson, K. Wårdell, and D. Loyd, *Analysis of temperature measurement for monitoring radio-frequency brain lesioning.* Medical & biological engineering & computing, 2001. **39**(2): p. 255-62.
65. Rao, S.S., *The Finite Element Method in Engineering*, 2011, Elsevier.
66. Kuntjoro, W., *An Introduction to the Finite Element Method*2005: McGraw-Hill Education.
67. Wårdell, K., P. Blomstedt, J. Richter, J. Antonsson, O. Eriksson, P. Zsigmond, A.T. Bergenheim, and M.I. Hariz, *Intracerebral microvascular measurements during deep brain stimulation implantation using laser Doppler perfusion monitoring.* Stereotact Funct Neurosurg, 2007. **85**(6): p. 279-86.
68. Hariz, M.I., P. Krack, R. Melvill, J.V. Jorgensen, W. Hamel, H. Hirabayashi, M. Lenders, N. Wesslen, M. Tengvar, and T.A. Yousry, *A quick and universal method for stereotactic visualization of the subthalamic nucleus before and after implantation of deep brain stimulation electrodes.* Stereotact Funct Neurosurg, 2003. **80**(1-4): p. 96-101.
69. Wilke, C.R. and P. Chang, *Correlation of diffusion coefficients in dilute solutions.* AIChE Journal, 1955. **1**(2): p. 264-270.
70. Reddy, K.A. and L.K. Doraiswamy, *Estimating Liquid Diffusivity.* Industrial & Engineering Chemistry Fundamentals, 1967. **6**(1): p. 77-79.
71. Sykova, E. and C. Nicholson, *Diffusion in brain extracellular space.* Physiol Rev, 2008. **88**(4): p. 1277-340.
72. Nicholson, C., *Diffusion and related transport mechanisms in brain tissue.* Reports on Progress in Physics, 2001. **64**: p. 815.
73. Nicholson, C. and J.M. Phillips, *Ion diffusion modified by tortuosity and volume fraction in the extracellular microenvironment of the rat cerebellum.* J Physiol, 1981. **321**: p. 225-57.
74. Abbott, N.J., *Evidence for bulk flow of brain interstitial fluid: significance for physiology and pathology.* Neurochemistry international, 2004. **45**(4): p. 545-52.
75. Nicholson, C. and M.E. Rice, *The migration of substances in the neuronal microenvironment.* Ann N Y Acad Sci, 1986. **481**: p. 55-71.
76. Miklavčič, D., N. Pavšelj, and F.X. Hart, *Electric Properties of Tissues*, in *Wiley Encyclopedia of Biomedical Engineering*, M. Akay, Editor 2006, John Wiley & Sons, Inc.
77. Gabriel, S., R.W. Lau, and C. Gabriel, *The dielectric properties of biological tissues: II. Measurements in the frequency range 10 Hz to 20 GHz.* Physics in medicine and biology, 1996. **41**(11): p. 2251-69.
78. Cheng, D.K., *Field and wave electromagnetics*. The Addison-Wesley series in electrical engineering1989, Reading, Mass.: Addison-Wesley. xvi, 703 p.

79. Audreccetti, D., R. Fossi, and C. Petrucci, *Dielectric properties of body tissue.* Italian National Research Council, Institute for Applied Physics, Florence, Italy, 2005.
80. Johansson, J., *Impact of Tissue Characteristics on Radio-Frequency Lesioning and Navigation in the Brain : Simulation, experimental and clinical studies*, in *Department of Biomedical Engineering*2009, Linköping University: Linköping.
81. Åström, M., J.D. Johansson, M.I. Hariz, O. Eriksson, and K. Wårdell, *The effect of cystic cavities on deep brain stimulation in the basal ganglia: a simulation-based study.* J Neural Eng, 2006. **3**(2): p. 132-8.
82. Wårdell, K., E. Diczfalusy, and M. Åström, *Patient-Specific Modeling and Simulation of Deep Brain Stimulation*, in *Patient-Specific Modeling in Tomorrow's Medicine*, A. Gefen, Editor 2011, Springer Berlin: Heidelberg.
83. Rice, M.E. and C. Nicholson, *Diffusion characteristics and extracellular volume fraction during normoxia and hypoxia in slices of rat neostriatum.* J Neurophysiol, 1991. **65**(2): p. 264-72.
84. Cragg, S.J., C. Nicholson, J. Kume-Kick, L. Tao, and M.E. Rice, *Dopamine-mediated volume transmission in midbrain is regulated by distinct extracellular geometry and uptake.* J Neurophysiol, 2001. **85**(4): p. 1761-71.
85. Lewis, G.A., D. Mathieu, and R.T.L. Phan, *Pharmaceutical experimental design*. Drugs and the pharmaceutical sciences1999, New York: Dekker. vi, 498 p.
86. Kirkwood, B.R. and J.A.C. Sterne, *Essential medical statistics*. 2nd ed2003, Malden, Mass.: Blackwell Science. x, 501 p.
87. Morel, A., *Stereotactic Atlas of the Human Thalamus and Basal Ganglia*. 1 ed2007: Informa Healthcare, New York, USA.
88. Bungay, P.M., P.F. Morrison, and R.L. Dedrick, *Steady-state theory for quantitative microdialysis of solutes and water in vivo and in vitro.* Life Sci, 1990. **46**(2): p. 105-19.
89. Chefer, V.I., A.C. Thompson, A. Zapata, and T.S. Shippenberg, *Overview of brain microdialysis.* Curr Protoc Neurosci, 2009. **Chapter 7**: p. 7.1.1-7.1.22.
90. Bungay, P.M., P.F. Morrison, R.L. Dedrick, V.I. Chefer, A. Zapata, and H.C.W.a.T.I.F.H.C. Ben, *Chapter 2.2 Principles of quantitative microdialysis*, in *Handbook of Behavioral Neuroscience*2006, Elsevier. p. 131.
91. Hardman, C.D., J.M. Henderson, D.I. Finkelstein, M.K. Horne, G. Paxinos, and G.M. Halliday, *Comparison of the basal ganglia in rats, marmosets, macaques, baboons, and humans: volume and neuronal number for the output, internal relay, and striatal modulating nuclei.* The Journal of comparative neurology, 2002. **445**(3): p. 238-55.
92. Rice, M.E., G.A. Gerhardt, P.M. Hierl, G. Nagy, and R.N. Adams, *Diffusion coefficients of neurotransmitters and their metabolites in brain extracellular fluid space.* Neuroscience, 1985. **15**(3): p. 891-902.
93. Lazar, M., D.M. Weinstein, J.S. Tsuruda, K.M. Hasan, K. Arfanakis, M.E. Meyerand, B. Badie, H.A. Rowley, V. Haughton, A. Field, et al., *White matter tractography using diffusion tensor deflection.* Human brain mapping, 2003. **18**(4): p. 306-21.
94. Shimony, J.S., R.C. McKinstry, E. Akbudak, J.A. Aronovitz, A.Z. Snyder, N.F. Lori, T.S. Cull, and T.E. Conturo, *Quantitative diffusion-tensor anisotropy brain MR imaging: normative human data and anatomic analysis.* Radiology, 1999. **212**(3): p. 770-84.
95. Sykova, E., J. Svoboda, J. Polak, and A. Chvatal, *Extracellular volume fraction and diffusion characteristics during progressive ischemia and terminal anoxia in the spinal cord of the rat.* Journal of cerebral blood flow and metabolism : official journal of the International Society of Cerebral Blood Flow and Metabolism, 1994. **14**(2): p. 301-11.
96. DeLong, M.R. and T. Wichmann, *Circuits and circuit disorders of the basal ganglia.* Archives of neurology, 2007. **64**(1): p. 20-4.
97. Åström, M., E. Tripoliti, M.I. Hariz, L.U. Zrinzo, I. Martinez-Torres, P. Limousin, and K. Wårdell, *Patient-specific model-based investigation of speech intelligibility and movement during deep brain stimulation.* Stereotact Funct Neurosurg, 2010. **88**(4): p. 224-33.

98. Kuncel, A.M., S.E. Cooper, and W.M. Grill, *A method to estimate the spatial extent of activation in thalamic deep brain stimulation.* Clinical neurophysiology : official journal of the International Federation of Clinical Neurophysiology, 2008. **119**(9): p. 2148-58.
99. Molinuevo, J.L., F. Valldeoriola, E. Tolosa, J. Rumia, J. Valls-Sole, H. Roldan, and E. Ferrer, *Levodopa withdrawal after bilateral subthalamic nucleus stimulation in advanced Parkinson disease.* Archives of neurology, 2000. **57**(7): p. 983-8.
100. Limousin, P., P. Krack, P. Pollak, A. Benazzouz, C. Ardouin, D. Hoffmann, and A.L. Benabid, *Electrical stimulation of the subthalamic nucleus in advanced Parkinson's disease.* The New England journal of medicine, 1998. **339**(16): p. 1105-11.
101. Zsigmond, P., M. Nord, A. Kullman, E. Diczfalusy, K. Wårdell, and N. Dizdar, *Neurotransmitter levels in basal ganglia during levodopa and Deep Brain Stimulation treatment in Parkinson's Disease.* In Manuscript.